REPUBLIC OF TURKEY
ACIBADEM MEHMET ALI AYDINLAR UNIVERSITY
INSTITUTE OF HEALTH SCIENCES

STUDIES OF MOLECULAR DYNAMICS SIMULATIONS AND BINDING FREE ENERGY CALCULATIONS ON THE AURORA A / N-MYC COMPLEX TOWARDS ELUCIDATION OF THE ROLES OF MYC BOX 0 OF N-MYC AND THE N-TERMINAL LOBE OF AURORA A IN THE BINDING EVENT

PINAR ALTINER

MASTER THESIS

DEPARTMENT of BIOSTATISTICS and BIOINFORMATICS

SUPERVISOR:
Assoc. Prof. Emel TİMUÇİN

ISTANBUL – 2021

REPUBLIC OF TURKEY
ACIBADEM MEHMET ALI AYDINLAR UNIVERSITY
INSTITUTE OF HEALTH SCIENCES

STUDIES OF MOLECULAR DYNAMICS SIMULATIONS AND BINDING FREE ENERGY CALCULATIONS ON THE AURORA A / N-MYC COMPLEX TOWARDS ELUCIDATION OF THE ROLES OF MYC BOX 0 OF N-MYC AND THE N-TERMINAL LOBE OF AURORA A IN THE BINDING EVENT

PINAR ALTINER

MASTER THESIS

DEPARTMENT of BIOSTATISTICS and BIOINFORMATICS

SUPERVISOR:
Assoc. Prof. Emel TİMUÇİN

ISTANBUL – 2021

DECLARATION

I declare that; this thesis study is solely my original work. I had no unethical behavior at any stage, from planning to writing; I obtained all the information in this thesis following academic and ethical rules, I have shown all the resources I have used in the bibliography. There is no violation of any patents and copyrights.

17/03/2021

Pınar Altıner

ACKNOWLEDGMENTS

First of all, my most valuable mentor, who is much more than a supervisor and, gave me the most incredible support during my master's degree. Also, she is the most tolerant advisor that a student can have. Thank you very much to Assoc. Prof. Emel Timucin. Then, I would like to thank everyone, especially Narod Kebabcı, who are Timucin Lab members, for their help.

Moreover, I would like to thank a jury member of my thesis are Prof. Dr. Osman Uğur Sezerman, Assoc. Prof. Emel Timuçin, and Assoc. Prof. Ahmet Can Timuçin, for their worthy contributions.

On the other hand, I would like to thank all my friends with whom we shared the same office for three years for their mental and guide support. Our comprehensive journal clubs, and scientific boosting have become valuable for me during this period.

Furthermore, I would like to thank my nearest and dearest partner, and my confidant to Rüçhan. It encouraged me to move to this field that I want to work on in life. He has been more than just a partner in our entire life. Thank you very much for everything.

Finally, I would like to give a huge appreciation to my family that has brought me up to this day and has done their best. I want to express my gratitude to my mother, Nilgün, and my father, Kurtuluş, who supported me in all my decisions and gave me the most significant financial and moral support in all difficulties.

TABLE OF CONTENTS

LIST OF ABBREVIATIONS AND SYMBOLS

AurA	Aurora Kinase A
LCPO	Linear Combinations of Pairwise Overlaps
MD	Molecular Dynamics
MM	Molecular Mechanics
MM-GBSA	Molecular Modelling - Generalized Born (GB) solvation model
NPT	Constant Number of atoms, Pressure, and Temperature
PCA	Principal Component Analysis
PDB	Protein Data Bank
PME	Particle mesh Ewald
QM	Quantum Mechanics
RMSF	Root Mean Square Fluctuation
RMSD	Root Mean Square Distance
SMILES	Simplified Molecular Input Line Entry System
TPX2	Targeting Protein for Xklp2

LIST OF FIGURES

LIST OF TABLES

SUMMARY

The currently published Aurora A/N-Myc complex structure (PDB-ID: 5G1X) states that the complex formation enhances the stability of N-Myc in cancer types where it is highly expressed. As N-Myc overexpression is frequently found in particularly neuroblastoma, targeting to inhibit this complex may be a valid strategy to decrease N-Myc levels. Although AurA has many inhibitors, which currently have already been used in cancer treatment, these inhibitors have a limited effect on tumors characterized by N-Myc amplification. The main reason for that N-Myc binds to AurA between the activation segment and the C-terminal lobe, while all AurA inhibitors are targeted to the ATP binding pocket. Therefore, AurA activity is not essential for interaction with N-Myc. 5G1X complex consists of two MYC boxes (MB) motifs. Although the structure is contained two motifs in the crystallization experiment, only the coordinates of the MBI structure were obtained. Besides, MB0 was reported as unmodeled in the PDB. Therefore, to prevent this characteristic interaction, designing molecules that directly target the AurA/N-Myc binding surface is a unique and original strategy to trigger N-Myc degradation. We aim to investigate the effects of structural alterations of AurA with currently known small chemical inhibitors on N-Myc binding. Therefore, MD simulations of all studied complexes were generated through 500ns. In this study, we also conclude that the interaction with TPX2 protein, a known partner of AurA, as well as directly analyzing the 5G1X complex with molecular dynamics simulations to evaluate the stability of the complex with a crystallized MB motif.

Keywords: Crystallization, Free Energy Calculation, Molecular Dynamics Simulation, N-Myc, Oncogene, Protein-Protein Interaction.

ÖZET

Bağlanma Olayında N-Myc'in Myc Box 0 ve Aurora A'nın N-Terminal Lobunun Açıklanmasına Yönelik Aurora A / N-Myc Kompleksi Üzerinde Moleküler Dinamik Simülasyonları ve Bağlanma Serbest Enerji Hesaplamaları

Kısa süre önce elde edilen Aurora A/N-Myc kompleks yapısı (PDB No: 5G1X). kanser hücrelerinde yüksek ifade edilen N-Myc kararlılığını artıran bir kompleks olarak önce çıkmıştır. Bu kompleks partnerlerinden AurA'yı hedefleyen çok sayıda inhibitör mevcut olmasına rağmen, bu inhibitörlerin N-Myc amplifikasyonu ile karakterize edilen tümörler üzerinde sınırlı etkiye sahip oldukları görülmektedir. Bu durumun sebepleri arasında, AurA/N-Myc bağlanma yüzeyinin katalitik bölgeden farklı bir bölgede olması ve AurA aktivitesinin N-Myc ile etkileşmesinde herhangi bir rol üstlenmemesi sayılabilir. Bu nedenle, AurA/N-Myc bağlanma yüzeyini doğrudan hedefleyecek moleküllerin tasarlanması, tümör oluşumuna artıran N-Myc'nin yıkımını tetiklemek için orijinal bir stratejidir. 5G1X kompleksi, iki MYC kutu (MYC boxes (MB)) motifinden oluşmaktadır. Kristalizasyon deneyindeki yapı her iki motifi de içerse de, sadece MBI yapısına ait koordinatlar elde edilirken MB0, yapıda modellenmemiş olarak raporlanmıştır. Bu sebeple, AurA'nın bilinen ve hali hazırda kullanılan ligandlarla olan yapısal değişimlerin N-Myc bağlanmasına etkisini araştırdık. Bu çalışmada, 5G1X kompleksini, kristalize bir MB motifi ile kompleksin stabilitesini değerlendirmek için moleküler dinamik simülasyonları ile doğrudan analiz etmenin yanı sıra AurA'nın bilinen bir partneri olan TPX2 proteini ile olan interaksiyonunu da bu çalışmaya dahil ettik.

Anahtar Sözcükler: Kristalizayon, Moleküler Dinamik Simülasyonu, N-Myc, Onkogen, Protein-Protein Etkileşimi, Serbest Bağlanma Enerjisi Hesaplaması

1. BACKGROUND AND AIM OF THE STUDY

Kinases are essential enzymes that play crucial roles in many biological processes ranging from signal transduction to metabolism (1). More than 518 different kinases have been identified in the human genome (2). These enzymes phosphorylate to their targeted protein at the side chain of some specific amino acid consisting of Tyrosine, Serine, Threonine. (3). In the case of the dysfunctionality of the unique biological amplifier causes various pathological conditions such as cancer and inflammation (3,8). Therefore, there is still a hot-topic to target such kinases to regulate their protein level in cells via therapeutic strategies (9).

AurA is such kinase that belongs to the Serine/Threonine kinase protein family (10). Similar to many other kinases, AurA is found to be amplified level in many cancers such as neuroblastoma (11), ovarian (12), prostate cancer (13). Under normal circumstances, AurA is dephosphorylated by PP1 so that it is transformed into an inactive state; however, in some conditions, AurA might be protected from its degradation with the aid of its protein stabilizer. TPX2 is a known partner of AurA responsible for the activation and stabilization of AurA (14). Recently studies suggested that AurA has another stabilizing partner is N-Myc (11). In contrast to TPX2, AurA/N-Myc interactions have not been associated with any pathways yet. The main reason for their interaction is still unclear; however, it has been identified that AurA blocks the ubiquitination of N-Myc, preventing its binding to the E3 ubiquitin ligase SCFFbxW7 and thereby stabilizing N-Myc (11,15). N-Myc and TPX2 compete for AurA interaction, suggesting that they interact through an overlapping surface(11).

With this perspective here, I aimed to investigate their structural mechanism behind AurA / N-Myc complex interactions by using computational methods. For this purpose, intermolecular interactions in the 5G1X structure containing the AurA / N-Myc complex dissolved in November 2016 have been extensively studied in the structural mechanism behind this affinity. (11). Despite being such an influential structure, 5G1X has a missing N-Myc portion, namely MB0. Thus, the missing part was constructed by a comparative modeling algorithm. Then, to test two various AurA complexes with another protein partner binds to the same AurA surface with the MB0 motif is TPX2 (16). Lastly, a chimeric form of TPX2 and MBI is computationally modeled. In this way, the MBI fluctuations would be compared with TPX2, MB0, and crystal form. Consequently, the stability and dynamics of distinct AurA/N-Myc complexes with varying MB motifs were delineated, attempting to unravel the most critical interactions.

2. INTRODUCTION

2.1 Cancer

All living organisms, from microorganisms to primates, perform countless metabolic activities during the course of their lifespan (17,18). One of the fundamental activities commonly encountered in all organisms is cellular division, which under normal conditions serves to expand their masses from embryonic to cell development and bacterial invasion. Under such circumstances, in which division cannot be controlled via cell cycle progressions, result in cancer. (19,20).

According to the American Cancer Society (ACS) definition, cancer is defined as uncontrolled growth resulting in an enormous proliferation of cells (18,19). This situation might occur due to various abnormalities, particularly in the regulatory processes. For example, mutation-based changes in the expression levels of oncogenes and/or chromosomal instabilities would result in such outcomes (21–23). These malformations generally reveal apoptosis and tumor suppression inhibition or growth and differentiation against self-defense mechanisms (24,25). Depending on the position of the mutation, oncogenes could be divided into two categories. If the mutation is in the protomer region, it may result in upregulation of oncoproteins, while if it is in the exonic regions, the gene product may lose its function, which indirectly causes a self-defense mechanism. The normal function of tumor-suppressing proteins is to prevent the growth of cancerous cells through different pathways. However, having negative impact mutations on the proteins responsible for the restraining tumorigenesis fails to prevent these abnormal divisions. Henceforth, disturbed tumor suppression mechanism having cells effortlessly pass through checkpoints in the cell cycle. In the further stages of carcinogenesis, healthy cells undergo cellular devastation

and intracellular stress in the aftermath. This rapid holocaust may indirectly result in revealing defense against cancerous cells due to the homeostatic balance disruption. On the other hand, the upregulation scenario refers to proto-oncogenes so, its overexpression induces cancer. Growth factors and mitotic division inducer proteins are mainly involved in this category. With the domino effect, this abnormal increase is likely to eventually lead to the defect in cellular division control (26), underscoring the significance of inhibiting such over-expressed/over-active enzymes for therapeutic purposes.

2.1.1 MYCN

The MYCN (Neuroblastoma-Myelocytomatosis viral gene) is one of the three members of the Myc family found in the short arm of chromosome 2 (2p24.3), which encodes the N-Myc protein (27). This gene was first identified in 1983 when genomic amplification of a gene construct with high sequence similarity to MYC was reported in a group of human neuroblastoma cell lines (27). However, different types of cancer are reported to have MYCN or N-Myc amplification, particularly 20% of neuroblastoma cases known to have MYCN gene amplification (28–30). Unlike other family members, which are cellular MYC (which encodes C-Myc protein) and MYCL (which encodes L-Myc protein), MYCN is a gene involved in the development of neural crest in the embryonic cells within the nervous system (31,32). Typically, the expression of MYCN is markedly reduced in the mature tissue during embryogenesis (33). Unsurprisingly, as with the other family members, the expression level of the MYCN gene is strictly controlled. However, due to genomic amplification, chromosomal translocation, and/or mutagenesis in signaling pathways, N-Myc protein levels would increase to cause tumors with poor prognosis (34,35). Because MYC family proteins are directly implicated in the tumorigenesis processes of many different human cancers, these proteins are recognized as valid targets for cancer drug

discovery studies. Notwithstanding this recognition, a number of compounds directly targeting N-Myc is quite limited, indeed clinically zero. Like other Myc family members, N-Myc was also described as undruggable, mainly because of transcription factors (31). Even though transcription factors were accepted to be undruggable, they consist of 20% of all oncogenes (36,37). The main observations leading to this paradigm are connected with the structural characteristics and cellular locations of transcription factors. Except for those that are inducible by ligands, they do not have any enzymatic functions that can be facilitated to pharmacologically targetable strategy, so they lack this specific pocket region that cannot be detected directly. Therefore, they are not likely to be targeted by antibody-based treatment approaches that are difficult to access into the cell.

Myc family is a protein family of helix-loop-helix-zipper class, consisting of 3 different transcription factors with a length of between 364-464 aa. This family carries the transactivation domain (TAD) at the amino terminus and the domain responsible for DNA binding and dimerization (DBD) at the carboxyl terminus. Only 83 aa length of the DBD region has a stable 3-dimensional shape; all the other parts of Myc proteins are determined as intrinsically disordered using circular dichroism and NMR spectroscopy (38–40). Thus, the general instability of the Myc family structure also precludes it harder to detect directly in cells. Although they do not have a specific 3D structure, there is a bHLHZ motif in this family, but it cannot be explicitly targeted from these regions because they are highly sterically hindered (41). Even if direct targeting is quite problematic, it is feasible to indirectly target N-Myc (31,42). The prevention of the interaction between N-Myc and other proteins, which mostly play a critical role in the invasion of cancer, might be one of the strategies to inhibit N-Myc. Protein-protein interactions of the Myc family are formed by a particular part of their TAD domain (40,43,44), which is a highly conserved region and called Myc boxes (MB). There are 5 MBs, namely, MB 0-I-II-III-IV. Interestingly, these MBs are characterized not to have any ordered secondary/tertiary structure, i.e., disordered. However, in line with other intrinsically disordered proteins, these motifs can

temporarily adopt an ordered secondary structure while interacting with another protein (38–40). The MBs are not only responsible for protein-protein interaction but also, depending on this interaction, regulate the overall stability of Myc proteins. (45,46).

MYC family proteins form a heterodimer with another bHLHZ class Myc-Associated factor X (MAX) to bind double-stranded DNA (41). This Myc / MAX heterodimer is basically responsible for gene transcription by RNA polymerase II through binding to the E-box palindrome with the canonical sequence of CANNTG (47,48). Although the Myc-MAX dimerization site was targeted in some studies, the resulting compounds did not show any promise *in vivo* (31,42). In addition to this, in studies conducted in the last five years, a protein named OmoMyc with a length of 118 aa (~ 15 kDa) has been reported to target both MAX dimerization and DNA binding (49,50). Since OmoMyc is a challenging molecule for intracellular delivery (42), cell-penetrating peptides that mimic OmoMyc activity have also been produced (51). Apart from a few and yet clinically untested direct Myc inhibitors, no other compound has been identified to inhibit N-Myc levels in cells.

Under normal circumstances, the N-Myc levels are controlled by SCFFbxW7 is one of the E3 ubiquitin ligases, which triggers proteasomal degradation by ubiquitinated N-Myc at K48 position (52,53). Even though the ubiquitination, Aurora A kinase (AurA) blocks the SCFFbxW7/N-Myc interaction. Based on that, N-Myc stability is elevated. There is currently not any known pathway to clarify this unravel interaction between AurA/N-Myc. However, a recent crystallization study resolved the complex of AurA and N- Myc (PDB-ID: 5G1X). Otherwise, like other transcription factors, N-Myc is classified as undruggable. Thus, the approaches directly targeting transcription factors, including N-Myc, are inconclusive (54).

Here in this thesis, one of the crucial complexes of N-Myc, AurA/N-Myc, has been extensively studied in molecular dynamics studies to understand complex interactions. This complex is significant as it represents the only complex to be used as an indirect but viable target for reducing elevated N-Myc levels, particularly in neuroblastoma cells.

2.1.2 AURA

Aurora is one of the Serine/Threonine kinase families responsible for regulating the cell cycle progression (55). Three members of that family are Aurora A (AURA), Aurora B (AURB), and Aurora C (AURC), respectively that mainly expressed in the G2/M control-point (55,56). Following that, Aurora A (AURA) is associated (control) with centrosome maturation, chromosomal discrimination and, microtubule persistency (57–59). Amplification of AurA is mainly observed in neuroblastoma, lymphoma, breast, prostate, and colorectal cancer (60–63). Mainly, the accumulation of AurA originates from TPX2 (Targeting Protein Xklp2). Both are responsible for the progression of microtubules during mitosis (64).

TPX2 is primarily responsible for microtubule assembly and cellular growth (65,66). The first 43 residues of the N-terminal lobe of TPX2 binds to AurA, and Nuclear Localization Signal (NLS) motifs (66), which locate in between amino and carboxyl-terminal, enable the transportation in the cell via interacting with Importin-alpha (67). Lastly, TPX2 (Kinesin 5) domain is found in at C-terminal, which is specialized by interacting with Xklp2. Both are associated with the regulation in the M phase (14).

AurA stabilization and one of the activation mechanisms of AurA are triggered by TPX2 during mitotic division. Under normal conditions, both AurA and TPX2 degrade via the ubiquitination process by APC/C (anaphase-promoting complex/cyclostomes)(68). The binding of AurA is protected from the hydrogeneration of the phosphoryl group of 288T, which is essential for its catalytic activity by protein phosphatase 1 (PP1) (14). Therefore, AurA would remain at an amplified level in the cell to provoke microtubule activation (66). Implicitly, it contributes to boosting mitotic cascades. Their stabilization mechanism still is a hot-topic for drug-discovering studies targeting AurA inhibition (16). Accordingly, the crystal structure of TPX2 exists only a partial peptide, which is a bound form of AurA and Importin-alpha. The relation of TPX2 to this study is to the binding site of AurA, which MB0 motif of N-Myc binds to AurA at the same surface.

To understand protein-protein interactions of AurA firstly must be comprehended conformational forms. There are two autoactivation mechanisms defined in the literature: phosphorylated to THR288 residue in its activation loop or effectuates a dimer with TPX2 (69). As an alternative mechanism, intermolecular interactions with two AurA, having a phosphate group and other is not, constitute “swapped dimer form.” (70). Thr288 residue is mainly phosphorylated to generate protein activation, also rarely Thr287 and Thr288 double phosphorylated (71). Examine protein structure is a key to identifying each difference and similarities between the active and inactive conformation of AURA (unique rearrangements) (5,16,72).

The AurA consists of two main domains: the regulatory domain located in N-terminus and the C-terminus catalytic domain. The regulatory domain is highly conserved compared to other kinase families; however, the catalytic domain is not conserved in evolutionary progress (73). In between two domains, a flexible ATP binding cleft is placed. Activation loop (segment) starts from the beginning of DFG

motif (274-276) to APE (297-299) motif (in AURA is mutated evolutionary A297P) (3,74). The rest of these motifs, the HRD (254 to 256) domain, is responsible for performing catalytic activation. In an active state, it generates critical interactions with the DFG-motif in the state (75) Additionally, at the connection between amino and carboxyl-terminal, aligning up the side chains of four hydrophobic amino acids (185,196,254, and 275) also play a vital role in stabilizing the core of the protein (76). Consequently, the main strategies of small molecule inhibitors of AurA aim to hinder those specific interactions (77).

Depending on the targeting region of these inhibitors might be classified into two subgroups. The ones that bind the active form of kinases are mostly a phosphorylated version called type-I inhibitors. This type of inhibitor mainly targets ATP binding pockets. In their presence, the DFG motif has already been defined as an “in” state. However, type II inhibitors distinctly shift the DFG conformation from “in” to “out” (76). These generally enhance the inactive form of kinases such as dephosphorylated or unbound TPX2. Apart from all, another unstable conformation between DFG-in and out existed, which is called DFG-up. Some type-I inhibitors convert active kinases from DFG-in to this intermediate form(78).

Nonetheless, these inhibitors cannot prevent N-Myc amplification because they are not directly bound to the binding surface of the AurA/N-Myc complex. Likewise, currently, research states that the catalytic activity of AurA is directly ineffective in the destruction or stability of N-Myc (11). Accordingly, it was found that AurA and SCFFbxW7 compete for binding of N-Myc (11,15). Besides, inhibition of the surface of AurA at the N-Myc binding side might be a promising strategy to lead up proteasomal degradation. Naturally, there is not known any proven stabilization features of interaction with N-Myc that affect AURA structure are not known yet. In light of this unique interaction, designing small molecule inhibitors that prevent their

binding region might be a promising approach to degrade protein in neuroblastoma cells.

2.2 Computational Biology

In general terms, proteins are macromolecules that are consisting of amino acids (79). Besides, they orchestrate numerous metabolic events, and catalytic cascades like cellular transport and translation are only some of the few functions of proteins. Examining the structures of these macromolecules, which have such an essential role in biological regulation to find solutions for many diseases (79). Computational biology mainly focused on sequence-based and structural behaviors and mathematical simulations of proteins via computational techniques (81)(82). Before analyzing the dynamics of the biomolecules in their nature, the solvated system would be relaxed via both energy minimization and equilibration steps. After the relaxation steps are the representation of the movements of the protein in the specified physicochemical environment in the desired time interval. Thus, it has an important place, especially in protein studies, as an alternative approach to costly wet-lab studies (84). In addition to its mobility only within a certain time duration, it includes many different methodologies such as protein-protein interaction, small molecule inhibitor interaction, or examining the effect of known mutations, estimation of structures whose three-dimensional structure is unknown (85). In this study, model predictions of the regions with unknown three-dimensional structures reported as loss in crystallization studies were calculated. Besides, the N-Myc mimetic peptide design, which is our plan, will be used as a very effective method in terms of both cost and time savings for the peptide library to be created.

2.2.1 Molecular modelling and dynamics

The natural interactions of all atoms would be described by either molecular mechanics (MM) or quantum mechanics (QM) methods. From protein perspectives, those interactions could be either intermolecular or intramolecular. For both interactions, types are assumed as a term of energy. Quantum mechanics mainly obeys the ab-initio and semi-empirical approach, and it explains the total energy of the particles using the Schrödinger equation (86). However, molecular mechanics utilize classical physics, and it defines total energy as a summation of potential energies comprising all interatomic interactions (87). Therefore, in the MM approach, the potential energy is classified as covalent and non-covalent. Thus, covalent bond interaction consists of a bond, torsion, and angle energy modeled by Hooke's potential energy.

On the other hand, non-covalent is referred to as secondary interactions divided into two distinct categories depending on effective ranges. Coulomb potential (r-1) is small range interaction, and it refers to charge-charge interactions. Besides, Lenoard-Jones potential (r-6) is a long-range interaction, so that represents van der Waals interactions. For molecular dynamics, the computation of long-range interactions of large systems does not cost-efficient, especially in biomolecules. This problem was solved by Particle mesh Ewald (PME) method (88). With PME, long-ranged interactions are perceived as the contribution of the overall system via the same trend. Thus, small-range contributions calculate at real-space while long-range contributions compute at Fourier Transform.

After assessing the overall potential energy of the systems based on a suitable model, acting forces on each particle would be calculated as the derivative of potential energy. Several estimations of forces based on the potential energies cover all possible bonded and non-bonded parameters, bond types that define unique molecular geometry (83,89). Then, the acceleration of each atom would be predicted concerning Newton's Second Law. As a result, the potential energy of the system was computed via a unified force field. Afterward, via appropriate force field, the interpretation of the position and velocity of interacting atoms was precisely monitored with the incrementation of time in the case of initial coordinates, and the velocity of atoms was foreseeable. In this section, general basics of molecular modeling methods and fundamentals principles behind molecular dynamics simulations. Molecular dynamics simulations are performed as our backbone for understanding mechanistic approaches of all AurA interactions in this thesis.

3. MATERIALS AND METHODS

3.1 PDB Structures

There are 1524 different AurA structure entry are found in PDB. To analyze various conformations of AurA, the pool was created by selecting the number of AurA proteins in the PDB. Firstly, selection criteria are determined as typing to avoid uncertainty caused by Aurora B and C, other protein members of the Aurora family. Only X-ray structures of AurAs were also selected by typing the gene name "AURKA" in query. Therefore, a total of 173 various AurA crystals were elected. The detailed information about the characteristics of all AurA proteins is located in Appendix A. After gathering the AurA library, a principal component analysis (PCA) was assessed by the Bio3D package in R studio (90).

3.2 Structure Preparation and Modelling

All studied AurA crystals are extracted from PDB, whose identical numbers are 2WTV, 2WTW, 3E5A, 4J8M, 4JBQ, and 5G1X, respectively. Molecular dynamics simulation has been utilized to study the AurA complex interactions. These were placed in a cubic water box center and neutralized by adding K^+/Cl^- ions. Meanwhile, in 5G1X complex ADP, the phosphor-threonine (TPO) and crystal water molecules of AurA in the 288^{th} position were preserved as well as all ligands bound forms of AurA. The crystal structure with double phosphorylated residues (PBD-ID:2WTV at 287 and 288^{th}) is transformed into an unphosphorylated version by two-point mutation to understand the effect of phosphorylation on the activation segment. Some parts of

proteins, which could not be determined in crystallization studies, are computationally predicted by MODELLER. These are an interconnecting region of TPX2, MB0 motif of 5G1X, and activation loop of 2WTW. Additionally, there is one new model generated via merging with TPX2 and MBI via Discovery Studio software.

Furthermore, the resulting system has dimensions varied from 512 $Å^3$ to 1712 $Å^3$ (x, y, z) and consists of ~ 70,000 atoms in total. This system has been subjected to energy minimization in 10,000 steps with the conjugate gradient approach without any restrictions. Then, all systems were simulated using the GROMACS molecular dynamics algorithm with the CHARMM36 force field (Huang & MacKerell, 2013) with periodic boundary conditions at 310 Kelvin constant temperature and 1 atm constant pressure using NPT thermodynamic framework for 500 ns (Phillips et al., 2005). "Particle Mesh Ewald" (PME) total method was used for electrostatic energy calculation (Harvey and De Fabritiis, 2009). Inside the systems, water molecules are modeled with TIP3P (Price and Brooks, 2004). The trajectories obtained as a result of these simulations were evaluated by the root mean square displacement (RMSD) and vibrations (RMSF), intermolecular bonds contact map. After that, the all-complex trajectory analysis was stated that N-Myc in 5G1X has drastically fluctuated. To confirm this instability, the MD simulation of 5G1X crystal was replicated with stable protocols and a different MD algorithm called NAMD.

3.3 Trajectory Analysis

Root Mean Square Fluctuation (RMSF) is implemented in the TCL console of VMD. However, pairwise RMSD is visualized by the “MD-analysis” tool in python. Principal Component Analysis (PCA) included in PC loadings, and residue contributions were calculated via Bio3D package in R. With this package, the distance

between the carbon alpha atoms of AurA-AurA and AurA - their partner (MB0, MBI, TPX2, TPX2/MBI, MB0-I) were computed both the first and the last frame of their simulations. Therefore, differentiation between the first and last frames shows the intramolecular and intermolecular displacement of the complexes.

3.4 Binding Free Energy Predictions

The AMBER score uses the MM-GB / SA method with the traditional polyatomic AMBER force field for protein atoms and the general AMBER force field for ligand molecules. The interaction between ligand and protein is represented in the terms electrostatic and van der Waals energy. Their solvation energies of the complexes were assessed based on the Generalized Born (GB) solvation model. During the AMBER score calculation, the input coordinates and parameters of the complex, ligand, and receptor are defined to the system via a configuration file. Next, minimization is performed using the conjugate gradient method to remove wrong contacts. Then, MD simulation (Langevin dynamics at a constant temperature, NPT ensemble) and a brief minimization to obtain the final energy of the system. The AMBER score also allows flexibility of a portion of the receptor during MD simulations to reproduce "induced fit" and allow the ligand and the entire complex movement. An optimization protocol was prepared to determine the most appropriate combination of all the parameters. Total twenty-three different protocols were attempted then, constant temperature 300 K, dual GB model (as a solvation method), pre-MD energy minimization 2000 steps, post-MD energy minimization 1000 steps, MD step 5100, and all receptor and ligand set as movable. The final coordinate files (.pdb extension) of the already calculated trajectory complexes were given as input. In the final stage of the energy calculation, a surface area term is added to the system. This term is derived using a fast LCPO (Linear Combinations of Pairwise Overlaps) algorithm (Weiser et al., J. Comp Chem 1999). Finally, the AMBER score is calculated by this algorithm through the free binding energies of the ligand, receptor, and complex, respectively.

4. RESULTS

4.1 AurA Structures Found in PDB

We investigated the entire PDB to analyze the structural variation among AurA 3D structures. Totally 173 different PDB structures are extracted, and these structures, along with their important structural and sequential features, are listed in Appendix A. Since we comprehensively examined the dynamical characteristics of the protein segmentally, only proteins obtained by the X-ray crystallography method are selected from PDB. Overall, 173 structures are identified whose source organism is reported as homo sapiens (95.4%) and Mus musculus (4.6%) sequence similarity. The sequence length of the complexes ranges from 263 to 306 amino acids in length. Both C and N terminal portions are conserved; however, the activation loop, which is placed between 270^{th} to 290^{th} of amino acids, is varied. However, 157 different ligands have been found in this library; 47 of them are involved in adenosine molecule modifications (AMP, ADP, *etc.*). Similarly, some materials used in crystallization processes, such as glycerol, ethanediol, and neutralization ions, are included in this number. Besides, in small chemical inhibitors, (1~{R})-1-(4-ethoxyphenyl) ethanamine has the lowest molecular weight reported as 165.23 g/mol, while coenzyme A is determined as the largest molecules found as 767.534 g/mol. In conclusion, we aim to reveal the dominant dynamism in the inner domains of the AurA with all these aurora complexes via generating various types of AurA complexes.

4.2 Building Experimental Structure Ensembles for AurA in PDB

PCA explains all information in a multivariate numerical data set by reducing the dimensionality of variables with minimal loss (91). In this way, more processable data are obtained to understand significant differences in complex systems. In this term, we utilized this statistical method for revealing the total atomic mobility of AurA crystals with significant and collective variances. We examined all AurA conformations that are available in the PDB database. According to activation loop conformation, these conformations are divided into inactive, active, and missing. The AurA structures are reported in the PDB are only involved in the kinesin domain spanned 133rd to 389th residues. The activation segment is placed between N and C terminus and starts from the DFG-motif to the APE motif (A mutates to P with evolutionary progress.)(3). Rather than both N and C terminals, the region located between those motifs is highly variable. All crystals are extracted in the PDB database depending on their loop conformation. Totally 173 crystals are found then, the activation loop of 101 (58%) of them are reported as “missing” 59 (34%) of them are eligible to bind N-Myc; lastly, 13 (8%) of them have inactive loop conformation. Although they are present in the crystallized molecule, which is missing in such protein structures, the missing regions that cannot be verified in X-ray diffraction contain high flexibility and structural irregularities (92). Thus, the ring is a flexible region, and the allosteric changes may not be rigid, with or without the AurA inhibitors. In addition to these, the allosteric mobilities of the proteins are not specific to only ligand binding. The nature of the protein dynamics contains such different conformations without the ligands (93). As a result, this allosteric variety is not able to completely prevent N-Myc binding.

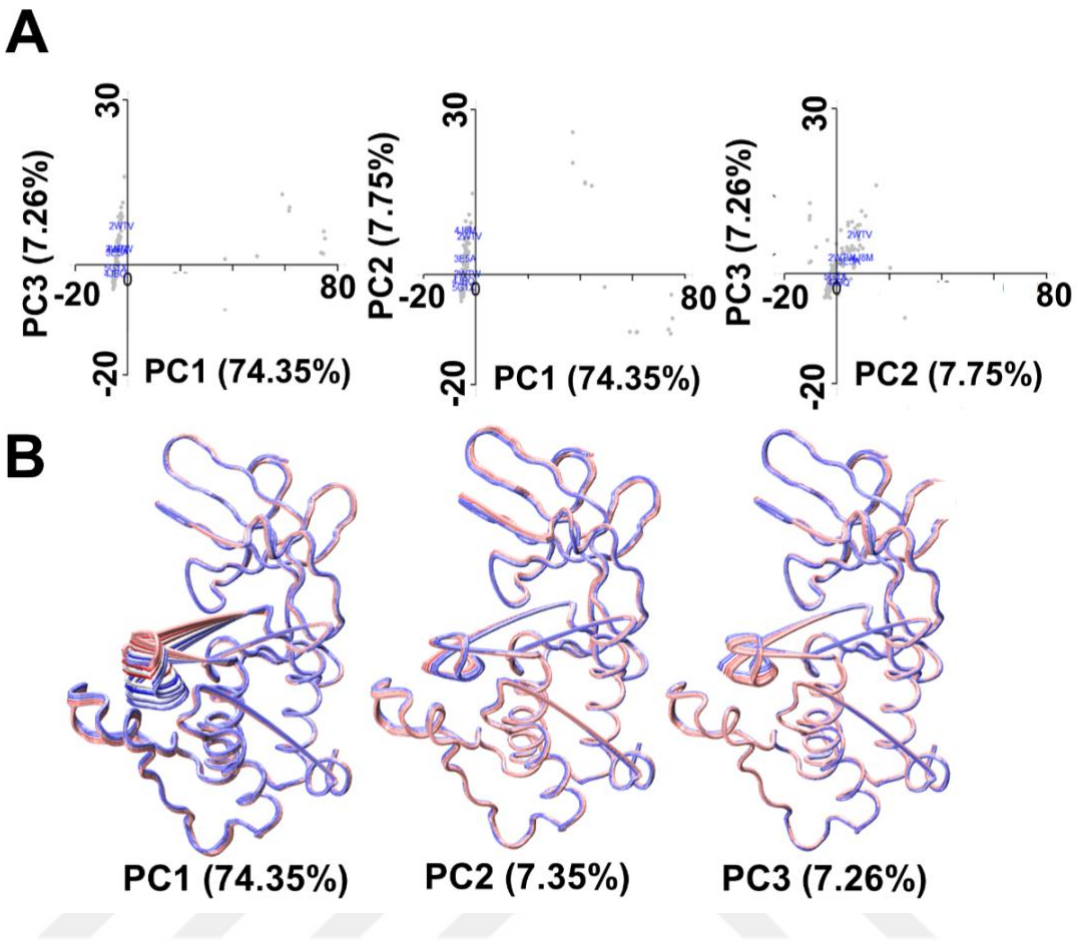

Figure 1. The first three PC results of PCA of constructed AurA proteins in PDB.

2D-PC loading plots of AurA crystals represented by gray points and the studied AurA crystals are indicated dark blue (1A). The residual contribution of each PCs is monitored by VMD via time scale coloring method (1B). From red to blue refers to movement direction.

To analyze the effect of the allosteric change in AurA on N-Myc binding, six different AurA structures are selected. A pool involved in currently reported all AurA crystals is generated to perform a principal component analysis of all 173 AurA crystals to detect significantly movable protein regions. Concerning the conformer plots of the structures are visualized by PC1 (74.35%), PC2 (7.75%), and PC3 (7.26%), which define all conformational differences dominantly (Figure 1A). Each point represents each AurA PDB-ID. The significant mobility is detected by PC1, whose scanning range is varied in -20 to +30 for most of the AurA crystals (Figure 1A). Thus, the AurA proteins that are investigated currently known all conformations are selected in that majority. Additionally, a significantly different movable region in the carbon

alpha atoms of AurA is generated depending on the first three PCs (Figure 1B). As shown in figure 1B, the activation loop region is dominated by all three PCs. Therefore, in this thesis, we examined all determined conformation of activation loops to accurately examine the effects on the N-Myc interaction.

4.3 Selected AurA structure for MD simulations

For activation of the region of AurA, there would be categorized in two distinct positions, and the ones one is a mirror image of the other with respect to its origin. Although all studied inhibitors in the thesis are targeted to the same region of AurA, which is ATP binding cleft, AurA tends to shift its activation segment via a catalytically inactive state depending on the specific ligand-protein interaction. Thus, in the alisertib-like ligand (PDB ID: 2WTV) and CD532 (PDB ID: 4J8M) bound to AurA activation loop rotate to the ATP binding cleft, which is called an inactive state. However, another inhibitor is VX6 (PDB-ID:4JBQ), and the different pose of alisertib-like ligand complex (PDB-ID 2WTW) are the opposite conformation which complexes are eligible to bind to AurA after reconstruction of all missing residues via computational tools. Therefore, the abundance of two distinct loop conformation in the same AurA inhibitor is shown that switching of the activation region could not be conserved due to thermodynamically non-spontaneous conformation. As a result, we have two distinct conformations of AurA with the same ligand, which are 2WTV and 2WTW.

In addition to these parameters, we removed PTM residues, which are primarily associated with protein activation, in a 2WTV crystal to emphasize the activation loop characteristics of the AurA protein. Consequently, with the combination of all these

inhibitors bound AurA crystals, we expected to analyze both types of currently known small molecule inhibitors that trigger to change catalytically active kinase conformation and the effects on phosphorylation of specific threonine residues (T287, T288) on the stabilization mechanism of AurA. Consequently, we mainly focused on the dynamic stability of that portion of AurA proteins because the MB1 portion of the N-Myc spanned throughout the activation segment of the AurA surface.

Table 1. Structural details about all studied AurA complexes.

Average numbers are represented by asterisk (*).

System	PDB-ID	Loop Conformation	Phosphorylated/Mutated Residues	Ligand	Partner 1 (Sequence Length)	Partner 2 (Sequence Length)	n	Time (ns)	Atom Number
AurA / N-Myc^{MBI}	5G1X	active	$^{T}288^{pT}$, $^{C}290^{A}$	ADP	AurA (264)	N-Myc^{MBI} (29)	4	500	38567*
AurA / N-Myc^{MB0}	5G1X	active	$^{T}288^{pT}$, $^{C}290^{A}$	ADP	AurA (264)	N-Myc^{MB0} (42)	1	500	29262
AurA / N-Myc$^{MB0\text{-}1}$	5G1X	active	$^{T}288^{pT}$, $^{C}290^{A}$	ADP	AurA (264)	N-Myc$^{MB0\text{-}1}$ (71)	1	500	38404
AurA / TPX2 / N-Myc^{MBI}	5G1X	active	$^{T}288^{pT}$, $^{C}290^{A}$	ADP	AurA (264)	TPX2 (37) / N-Myc^{MBI} (29)	1	321	62514
AurA / TPX2	3E5A	active	$^{T}288^{pT}$	VX6	AurA (264)	TPX2 (37)	1	473	60248
AurA	4JBQ	active	$^{T}288^{D}$	VX6	AurA (265)	none	1	500	64364
AurA	4J8M	inactive	$^{T}287^{D}$	CD-532	AurA (265)	none	1	500	36579
AurA	2WTW	active	$^{L}215^{R}$, $^{T}217^{E}$, $^{R}220^{K}$, $^{T}288^{pT}$	ZZL	AurA (262)	none	1	500	44775
AurA	2WTV	inactive	$^{L}215^{R}$, $^{T}217^{E}$, $^{R}220^{K}$, T287pT, $^{T}288^{pT}$	ZZL	AurA (263)	none	1	500	44775
AurA	2WTV	inactive	$^{L}215^{R}$, $^{T}217^{E}$, $^{R}220^{K}$	ZZL	AurA (263)	none	1	500	36662

Afterward, the 5G1X complex consists of two MYC box motifs though only MBI is validated, MB0 is unmodelled. Therefore, the missing portion of N-Myc is constructed so, the complete form of the 5G1X complex is obtained. Rather than this complete form, only the MB0/AurA complex is generated to analogize each MB region separately. In TPX2/AurA complex (PDB-ID:3E5A), we observed not only compare the binding affinity of the MB0 portion of N-Myc to the AurA but also showed the effects on the VX6 to AurA with or without TPX2.

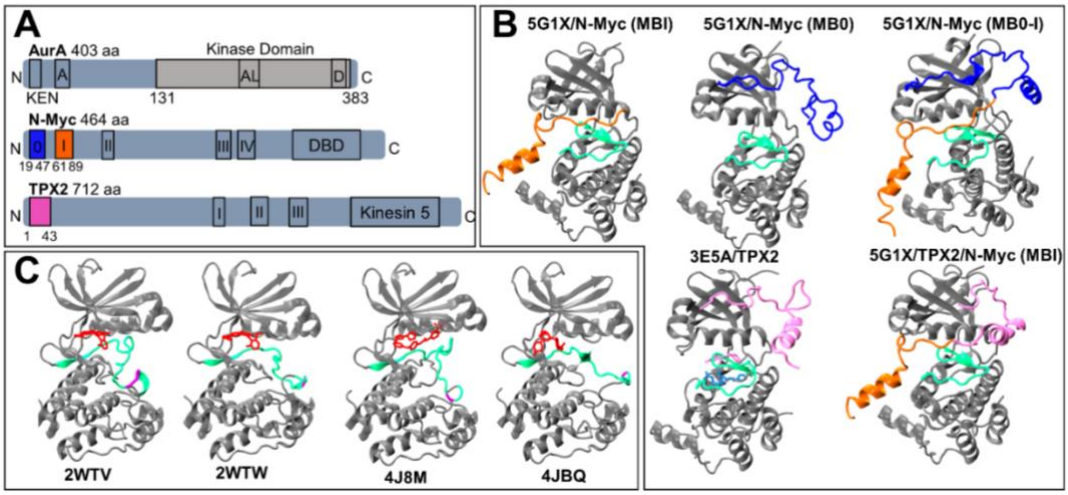

Figure 2. Structural characteristics of all studied AurA complexes.

Domain architecture of complex unit (2A). Protein partner and inhibitor bound complexes are demonstrated respectively. The activation segment also colored by light green, also phosphorylated residues are shown as magenta on this loop (2B,2C). All partners are colored with respect to Figure2A. Small molecule inhibitors are indicated by red (2C).

Lastly, a chimeric form of TPX2 and MBI is constructed. The reason for the evaluation of the chimeric model is to reveal that is the addition of the TPX2, any effects on changing MBI mobility rather than the elongated form of N-Myc. In this way, we compare the mobility of MB1 combined with TPX2, MB0, and solely MBI.

4.4 Structural Features for Probing AurA Activation and Stabilization

This section mainly focused on the fundamental interactions for kinase activation. All analyses are assessed both inhibitor and protein partner forms of the complexes separately to determine their enzymatic characteristics. Depending on the inactive features, the effects of AurA on the region associated with the protein interaction are

intensively studied, consisting of DFG and HRD motifs, hydrophobic spine and, specific salt bridge (E181-K162), respectively.

4.4.1. CHI angle displacement of aspartic acid and phenylalanine of DFG motifs

Kinase inhibitors are divided into different groups according to the target area. In the literature, among the small molecule inhibitors targeted to AurA, there are only type1 inhibitors whose crystal structure is currently available. Type1 inhibitors mainly target the ATP binding pocket. These ligands, developed to disrupt the AurA activity, have a desirable affinity for AurA, as well as disrupt the interactions that play a vital role in the self-stabilization of AurA. In this study, we investigated the effects of these critical interactions on the protein partner interactions of AurA in the ligand/AurA complexes, which have already targeted AurA and are undergoing phase studies.

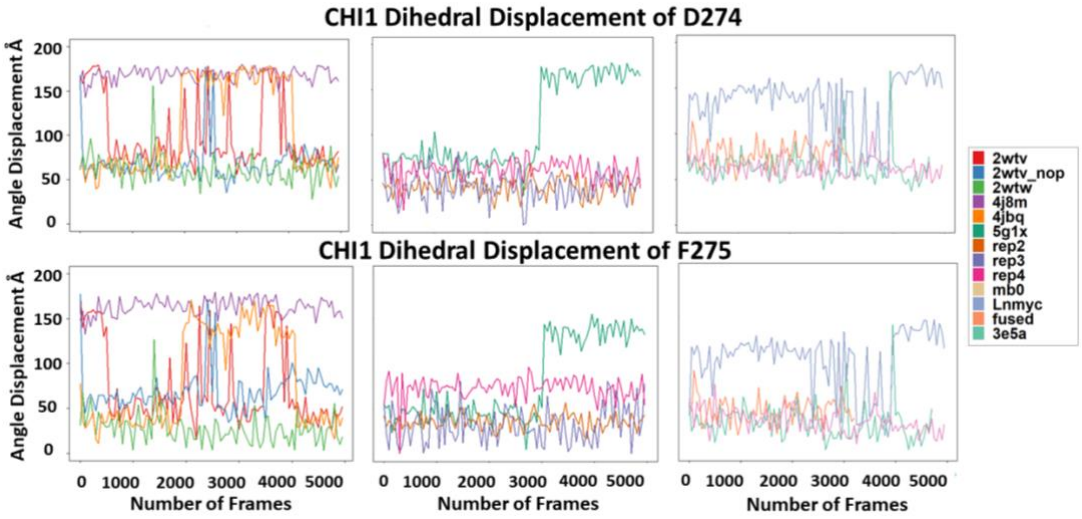

Figure 3. CHI angle displacement of D274 and F275 residues.

All 13 different AurA complexes are examined into 3 main plot that are consisting of inhibitior bound crystals, 5G1X replications and protein partner complexes respectively.

Additionally, the type I inhibitors also are divided into characters according to the conformational changes that occur in the DFG motif. AurA activity is categorized as DFG-in, up, and out. In the active form, the DFG motif is in conformation placed in D, and F's side chains look towards the ATP binding pocket. However, this characteristic position is deflected in DFG-up and out states by designed inhibitors. Accordingly, the movements of the CHI1 angles of both Asp and Phe residues, which are the side chain in the DFG motif, are analyzed along the simulation time. As shown in Figure 3, the angles of these amino acids are around 150 degrees between 200-400 ns at 4JBQ and, throughout the simulation, at 4J8M. While there are similar jumps in phosphorylated in 2WTV, there is no significant mobility seen in non-phosphorylated 2WTV compared to AurA inhibitor-bound structures. 2WTW also has a similar characteristic of the active forms of the AurA's, bound to the protein-partners are attached. Although both the constructed (5G1X/MB0, 5G1X/MB0-I, 5G1X/TPX2/MBI) and the crystal complexes (3E5A and 5G1X) which are interacted with protein, whose angles of Asp and Phe amino acids remained between 50-100 degrees during the simulation period, extreme rotations are observed in the first iteration of 5G1X and 5G1X/MB0-I structures. However, the mobility of these two

complexes concerning the CHI angles relatively fluctuates in the DFG motif; this fluctuation did not play a role in the interaction with the HRD motif, whose interaction is accepted as vital for the undergoing regulatory mechanism of the AurA. In addition to that, both the distance matrix and essential dynamical analysis show that the first replication of the 5G1X crystal has a fashionable place among other repetitions while the extended structure has increased its complex stability. These results show that the mobility of Asp and Phe amino acids in CHI aspects does not significantly impact the protein-protein interaction of AurA. Also, there is no sharp difference found between the inhibitor-bound AurA and protein-partners structures. Besides the side-chain rotations of Asp and Phe amino acids, we also included the interaction with the HRD motif, which is the motif responsible for catalytic activity, to examine the effect of inhibitors from a different perspective.

4.4.2. Distance distribution between the residues in DFG motif

In protein partner-bound AurA structures, the side chain of the His254 and Phe275 are faced to each other rather than inhibitor-bound complexes (Figure 4). To confirm this difference, we assessed the distance between their first carbon atoms of the side chains (Cγ) for thirteen complexes during their simulation time. As shown in Figure 4, the total displacement between these motifs is determined around 12 Å in both ZZL bound-AurA complexes regardless of their phosphorylation states. However, in the active loop of the same ligand, 2WTW performs similar behavior to the protein-partner bound complexes. Only the VX6 bound form of AurA (4JBQ) shows similar results for the CHI angle analysis, while in 4J8M did not affect the interaction between DFG and HRD motifs extreme CHI angle fluctuations DFG motif. Consequently, neither the interaction between those motifs nor DFG angle displacement did not give enough evidence that reveals the kinase activity.

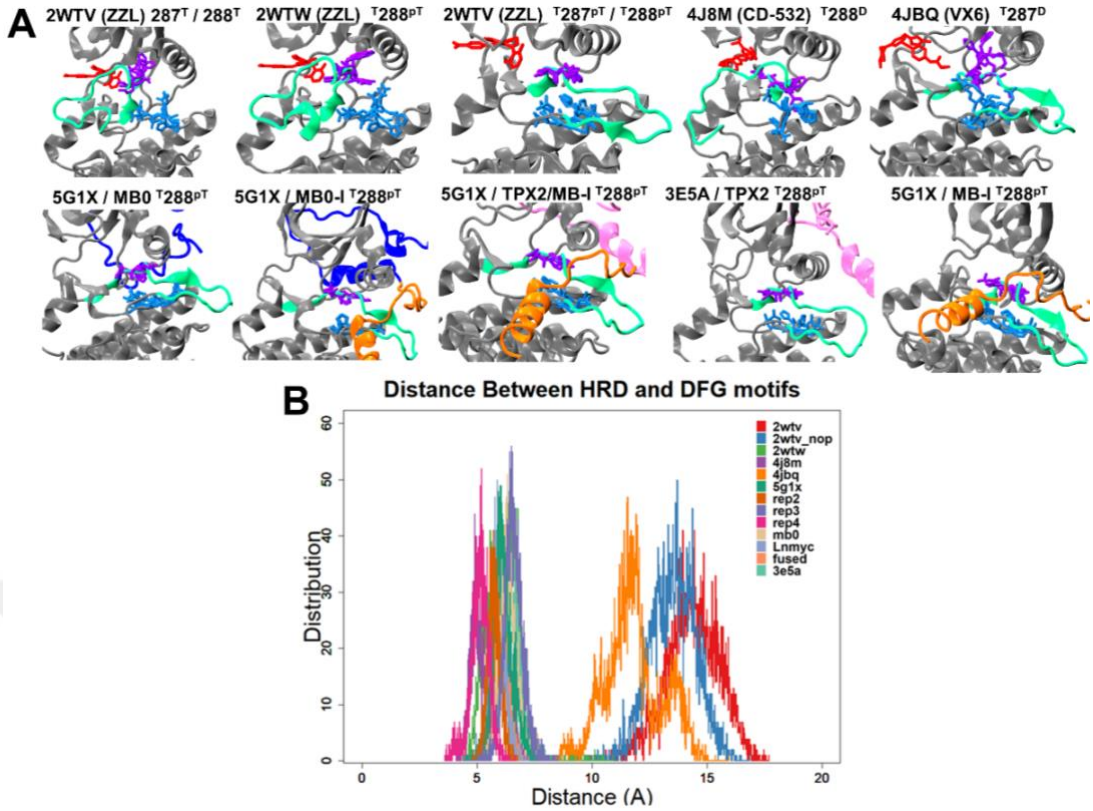

Figure 4. Distance analysis between E181 – K162 for all AurA complexes.

Conformational changes of DFG and HRD motifs are demonstrated during the simulation. The same coloring methods are used for all structural figures, however DFG and HRD motifs are represented licorice and colored purple and blue, respectively. (4A).
The distance between Cγ atoms between F275 and H254 are measured for each complex (4B).

4.4.3. Hydrophobic spine stabilization of all AurA complexes

Another essential interaction created by the dynamism of the DFG and HRD motifs is the desirable hydrophobic arrangement formed by the side chains of the accompanying residues. Phe275 in the DFG motif, His254 in the HRD motif, Lys196 in the β4 strand in the N-terminal lobe and, Gln185 in the αC helix domain, are generated this spin via hydrophobic stabilization. The protection of this spin is quite crucial for the self-stabilization of AurA. Therefore, the hydrophobic spine stabilization is analyzed to evaluate the effects on the conformational kinase

differentiations by taking a snapshot during their simulation time. Moreover, RMSF analysis is performed for all atoms of these spine residues to make a complete residue-specific analysis of the spin destabilization. As expected, side chains are relatively more hydrophobic and occupy a large region; the mobility in the side atoms of His254 and Phe275 is greater than the side chains of Leu196 and Gln185 residues. All mobility in Leu196 is almost the same in almost all structures. In Gln185, 4JBQ and 2WTV (T287pT, T288pT) showed the highest fluctuations in all atoms. On the other hand, 4J8M and 5G1X/MBI(n=4) also show the same mobility at OE1 and C atoms. Besides 4JBQ, the mobility of His254 residues is observed, in the protein partner-linked structures of AurA, especially in their side-chain atoms. Unlike the other three residues, the most extreme jump is seen in 2WTV (T287pT, T288pT). Still, leaping in the complexes where AurA performs other protein-protein interactions independent of MBI is observed in His254. In other aspects, the minimum mobility of 4J8M is also seen in His254. In Phe275, similar to the results of CHI1 angle displacement, the mobility of 4JBQ and 4J8M dominated the movements of all the remaining structures.

Aside from the RMSF results, the snapshots of the initial and the final step of the simulation, spine inhibition occurred in both phosphorylated and non-phosphorylated 2WTV complexes preserved throughout the simulation. In both 2WTW and 4JBQ structures, the first 200 ns of the simulation remain stationary, while the spine form is broken in the rest of their trajectories. Only 4J8M behaves like protein-partner AurA complexes, maintaining this hydrophobic backbone stably throughout the entire simulation. As a result, inhibitor-bound AurA structures are compared against each other, stabilization in the spin occurred regardless of either the loop position or the phosphorylation state. Despite some of the atoms with extreme jumps in RMSFs, this cluster is still preserved.

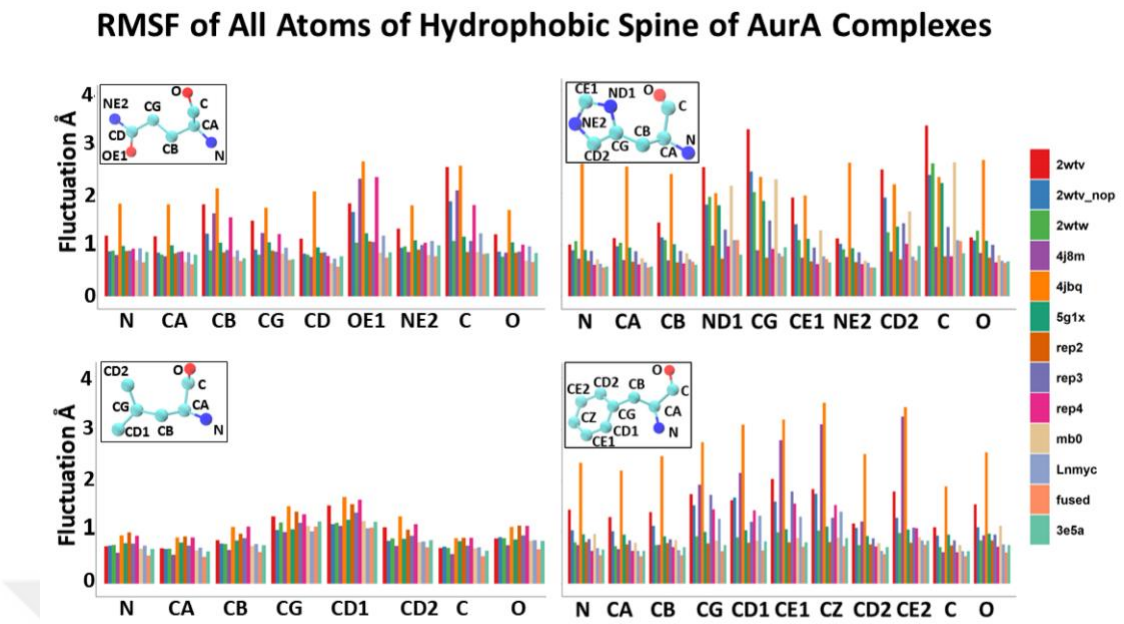

Figure 5. RMSF results of all atoms of hydrophobic spine residues.

Each bar graph is represented each residue are located in Gln185 (on the upper-left), Leu196 (bottom-left), His254 (upper-right), and Phe275 (bottom-right). Each nomenclature of atoms is shown each bar graph.

Furthermore, spin immobility is preserved in all AurA/partner complexes. Again, His254 and Phe275, which participated in the hydrophobic spine stabilization, and have the highest hydrophobicity in DFG and HRD motifs, did not observe possible to directly affect the distance N-Myc of MB0 part, which is the most critical portion in N-Myc. Because Leu196 is found in the β-strand of the N-lobe, and Gln185 is in the Cα motif, none of which are located on the binding site. The mobility in those regions may affect intermolecular binding. The drastic effect on the solely interacted form of VX6 (4JBQ) completely disappeared in the presence of TPX2 form (3E5A). A similar situation might also occur with N-Myc MB0-I binding in the presence of an inhibitor.

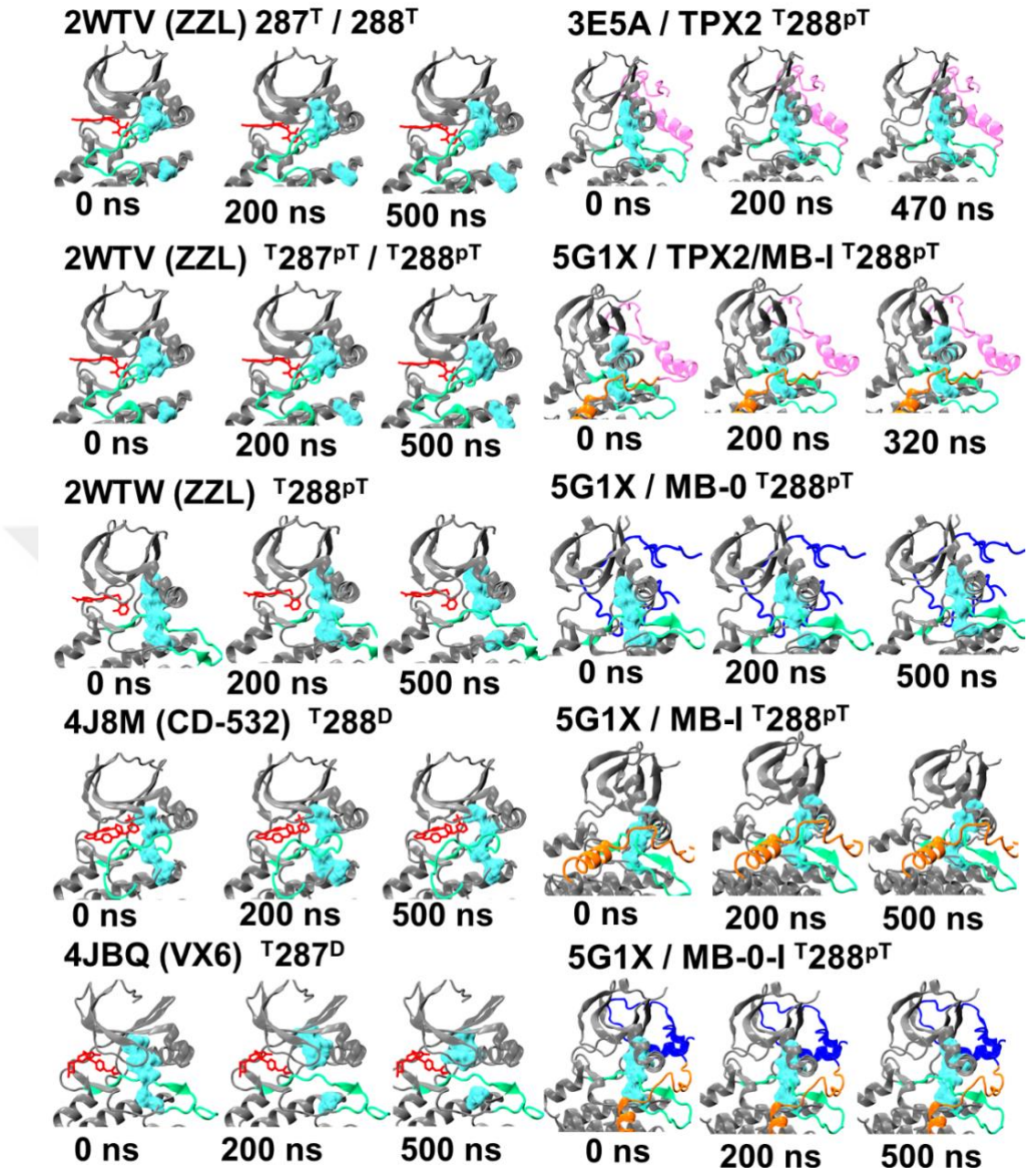

Figure 6. Hydrophobic spine rearrangements of all complexes at beginning, intermediate and final steps of simulations.

Hydrophobic clusters are represented by surface and colored by cyan.

4.4.4. Distance distributions of salt bridge between lysine 162 and glutamic acid 181

Last but not least, another key factor that plays a vital role in the kinase activity of the Serine/Threonine kinase family is placed in the β-3 strand in the Lysine and Cα helix in Glutamate residues in AurA. Since this interaction is found in the N-terminal lobe of the AurA, it has a certain significance rather than other interactions examined in this study. In ZZL bound having inactive loop conformation, show the highest fluctuation regardless of its phosphorylation states. Following that, 4JBQ and 4J8M that has a similar destabilized trend. In contrast to inactive loop forms of AurA (2WTV, 4J8M) and 4JBQ crystals, 2WTW behave in a particular character than all inhibitor-bound AurA structures. Together with the 5G1X and 3E5A crystals, this salt bridge remains a steady state in the constructed partner bonded structures. After the 3000^{th} frame of the simulation of the first and the fourth iteration of 5G1X crystals, there have been cases where the distance exceeds 5Å during the simulation period compared to the stable structures, emphasizing that the 5G1X structure alone is not stable shown in Figure7. In the third iteration of the same complex in which the AurA/N-Myc interaction is almost zero at the end of the MD simulation, the salt bridge is entirely preserved (Figure10). The MBI/AurA interaction may be caused by the irregular movements originating from the MBI in the overall complex. This result confirms our hypothesis that, in the presence of AurA N-terminal dominantly stabilizing structures such as MB0 and TPX2, AurA activity is the most optimal status.

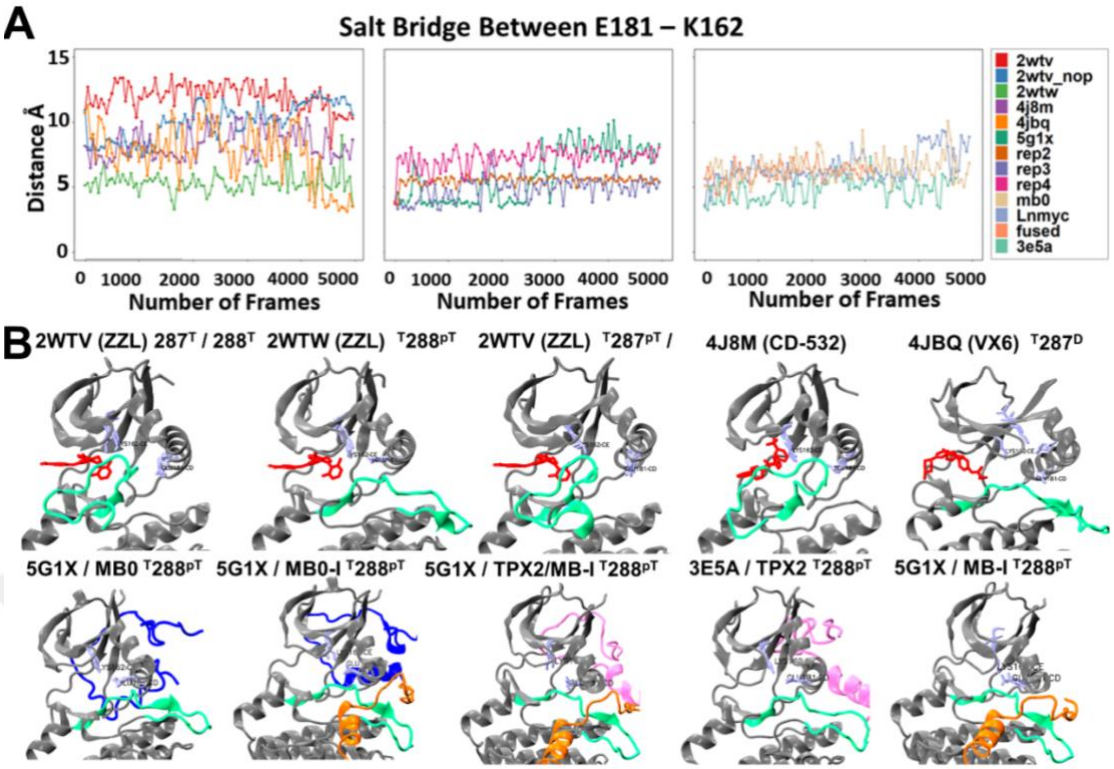

Figure 7. Salt bridge analysis between E181- K162.

All 13 different AurA complexes are examined into 3 main plot that are consisting of inhibitior bound crystals, 5G1X replications and protein partner complexes, respectively.

This static interaction located at the N-terminal lobe of the AurA is associated with kinase activity is protected in the presence of partners that bind to the same surface of the same AurA. Nevertheless, in the presence of VX6 with TPX2 completely loses its inhibitory effect. Then, in the 2WTW crystal, this interaction recovers due to the activation loop rotation compared to the 2WTV, which is the different crystal in the same study. If this salt bridge disturbs, the N-terminal region of AurA could become unfavorable for N-Myc binding. As a result, the inhibition of this salt bridge plays a crucial role in peptide design to prevent N-Myc interaction, targeting AurA.

4.5 Dynamical Fluctuations Analysis of AurA Complexes

In this section, structural mobility assessments of the AurA complexes are analyzed during the MD simulation, including pairwise RMSD, RMSF, PCA, and distance matrix differences, respectively.

.

4.5.1 Pairwise RMSD analysis

After completing the MD simulation, the Root Mean Square Distance (RMSD) of all complexes are calculated throughout the simulation time. 4J8M is the least fluctuated complex in the inhibitor bound AurA crystals during 500 ns in other respects, total distance deviations of 4JBQ reached 4-5 Å, especially during 0-200ns. In alisertib bound structures, which have inactive phosphorylated activation loop (2WTV), the deviations take during 200-400ns approximately 3-4 A. However, total fluctuations in the same complex the unphosphorylated form observed only 0-150ns. Interestingly, the active conformation of AurA with the alisertib-like inhibitor (2WTW) has a similar pattern of phosphor-mimic inactive form. These RMSD results show that the bound of CD-532 preserves overall stability independent of inactive conformation and phosphorylation. At least one phosphorylated threonine (either 287 or 288) residue is vital for conserving the complex mobility as active loop conformation for inactive alisertib complexes. Even if 4JBQ has the same phosphorylation state and loop conformation as 2WTW, VX6 destabilizes AurA more effectively. With the interaction between TPX2 and AurA-VX6 complex (3E5A), complex mobility is reduced. None of them has as low RMSD as the 3E5A complex in other protein-partner complexes though having AurA inhibitors. Especially, AurA/N-Myc crystal (5G1X) has the highest RMSD score in 4 repetitions. However,

in the elongated form of this complex, its RMSD is decreased drastically. Subsequently, it observed higher stability by replacing MB0 with TPX2. Similar to TPX2/MB1 complex, only MB0 of the N-Myc bound AurA structure also shows lower complex fluctuation rather than 5G1X crystal. Considering all these pieces of evidence, AurA dominantly generates protein-protein interaction in the C-alpha helix (residue number from 170 to190) that is the binding site of TPX2 and MB0. Solely, MB1 of N-Myc/AurA interaction could not be enough for their stabilization.

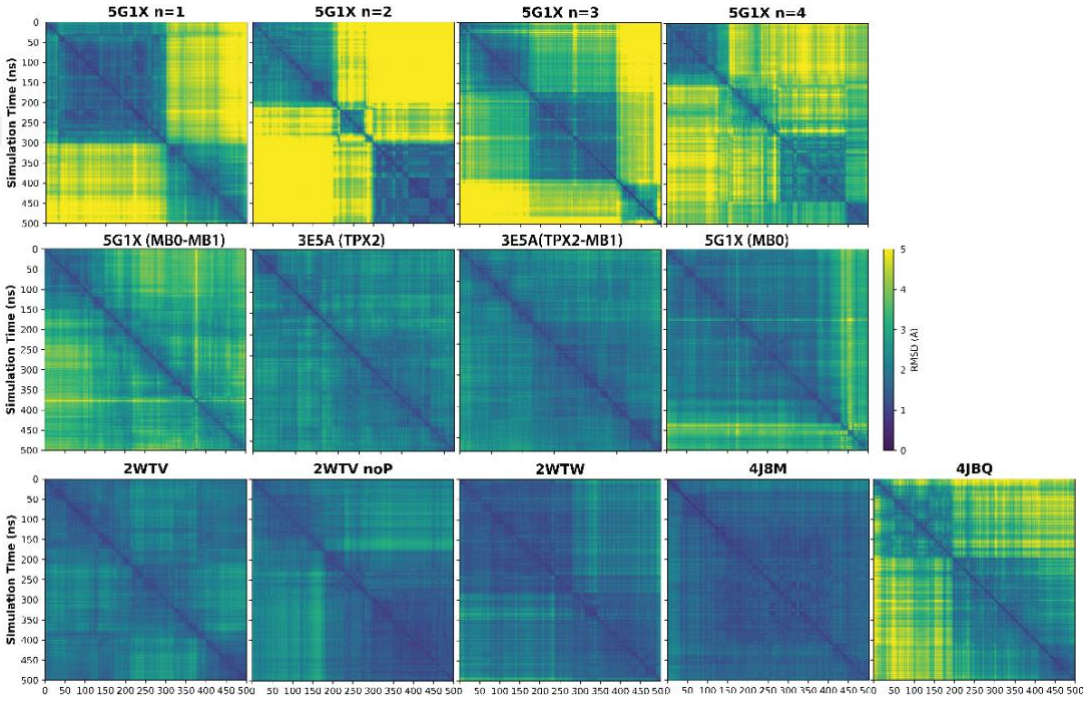

Figure 8. All to all RMSD results of all complexes.

4.5.2 RMSF analysis

To identify the effectivity of residue-wise contributions on the RMSD result, the Root Mean Square Fluctuation (RMSF) of each complex is calculated. Except for the activation loop region, the highest fluctuations belong to 4JBQ for all residues of

AurA. The fluctuation in the activation loop dominates the overall difference in inhibitor-bound aurora structures. Three various forms of ZZL bound complexes are analyzed depending on phosphorylation state and loop conformation. The 2WTV complex has an inactive and unphosphorylated state; its deviation reached approximately 7 Å at the activation loop. Even if 4J8M is also the same characteristic, its loop mobility only increases as half of the same states of 2WTV due to phospho-mimic mutation that is T288D. Surprisingly, in the double phosphorylated inactive form (2WTV), loop mobility shifts nearly ten amino acids throughout the N-terminus. It is still the most stable loop after the 4J8M. By comparing active inhibitor-linked AurAs, it has shown that VX6 does not only destabilize the activation loop but also has a higher RMSF value than across all ZZL bound AurA residues (2WTW).

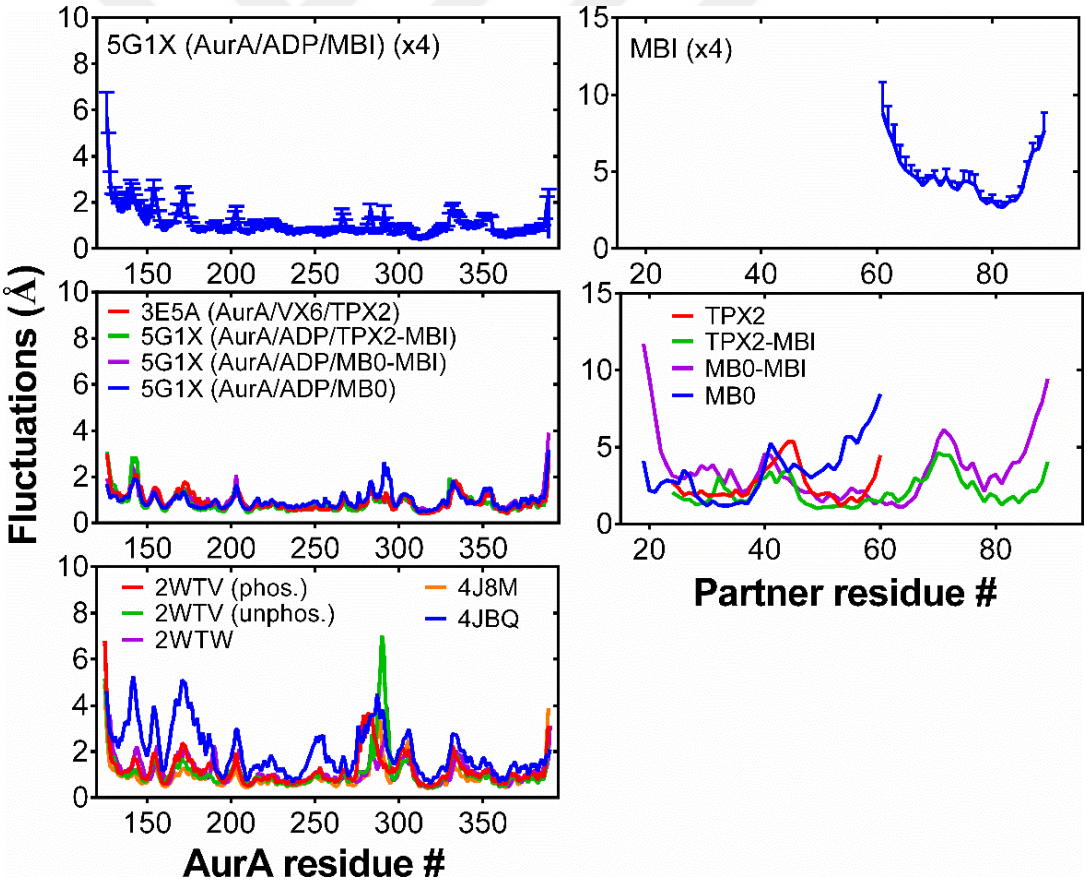

Figure 9. RMSF results of all AurA and its protein partners.

As expected, inhibitors bound AurA complexes to have higher RMSF than bound to binding partners. The distinct difference between inhibitor-bound and protein partners bound of AurA structures is the fluctuation on the activation loop is lower and divaricated. In other aspects, all repetitions of 5G1X have observed extreme fluctuations, especially in N and C terminals of AurA rather than whole systems. By inserting MB0 to MBI, AurA achieved the most stable loop and N-terminal forms against the rest of the systems. However, only MB0 is insufficient to stabilize the AurA complex as much as MB1 (5G1X). AurA/MB0 interaction is most prominent in reducing the fluctuations in the N-terminal region of AurA. Nevertheless, mobility in the loop region and C-terminal is more remarkable than other protein complexes. In between 138-148th amino acids (β1 and β2 of AurA) where MB0 and TPX2 interacting zone of AurA, it has seen as an extreme deviation only at that portion of AurA in contrast to TPX2/AurA (3E5A) and MB0-AurA that show desirable stabilization. Except for that, a similar trend is observed in AurA by appending MB1 to the TPX2.

Moreover, the mobility of the partners during the simulation time in the complex is critical for discussing their binding affinity to AurA. In two out of four repetitions of 5G1X, N-Myc partially dissociated from the complex. Likewise, the rest of them also are not capable of sustainable interaction. Although with the elongation of MBI to the N-terminal (MB0-MBI), waving of N-Myc is drastically decreased, both terminal regions are still not contributing to complex stabilization. Solely MB0 could eliminate N-terminal fluctuation. Otherwise, the average mobility of MB0 is exceeded to 5 Å after the 40th residue. Actually, at the position, all of the AurA partners show extreme jumps.

Meanwhile, fusion form and 5G1X/MB0-I and 3E5A slightly conserve their stabilities at the interconnecting region (between 50-60th residues). MBI portions of both 5G1X TPX2/MBI and 5G1X MB0-I complexes show similar characteristics to

5G1X MBI complexes. While both forms of MB0 complexes interacted with AurA via mainly 29-39th and 49-59th residues of MB0, there is no distinct contribution to the complex stabilization, especially from the 19th to 29th residues of MB0. However, at the C terminus of the TPX2 is barely interacted with AurA (PDB-ID: 3E5A); those parts contribute to complex stabilization after MBI construction to the TPX2. Consequently, with the addition of TPX2, the MBI fluctuations are changed in a positive manner. Also, MBI contributes parts of TPX2 that do not interact with AurA to the complex stability.

4.5.3. Trajectory based PCA analysis

Principal component analysis (PCA) might be summarized as explaining all information in a multivariate numerical data set by reducing the dimensionality of variables with minimal loss. In this way, more processable data are obtained for an understanding of major differences in complex systems. In terms of our study, we utilized this statistical method for revealing the total atomic mobility of AurA and its complexes throughout the simulation time with significant and collective variances. For all 13 structures, six variances are captured by each PC. From these PCs, the conformer plots of the structures are visualized by PC1 and PC2, defining all conformational differences dominantly. Each point represents each number of frames. Therefore, there is no confined cluster in all iterations of 5G1X except the blue one. Otherwise, some portion of the repeats is clustered in PC1 at a common point extending to -50. However, such conformers found in neither inhibitor-bound nor partner-bound AurA complexes have been observed, especially in green and purple repeats. It proves that 5G1X is not stable throughout its trajectories depending on both having a primary conformational range and not having a distinct grouping within themselves than other structures. A similar amount of co-clustering at 5G1X is observed in L-Nmyc, but the rest of the clusters in L-Nmyc are shaped on PC2

variability in the range of -50 to +50. The major MB0 structure grouping corresponds to the original offset of the green 5G1X model. In the minor part, there is a 50 unit shifting in the negative direction from PC1 and in the positive direction from PC2. Fusion and TPX2 complexes showed lower displacement than other combinations of nmyc. Their pattern is that it does not exceed 50 units in both PC1 and PC2 axes.

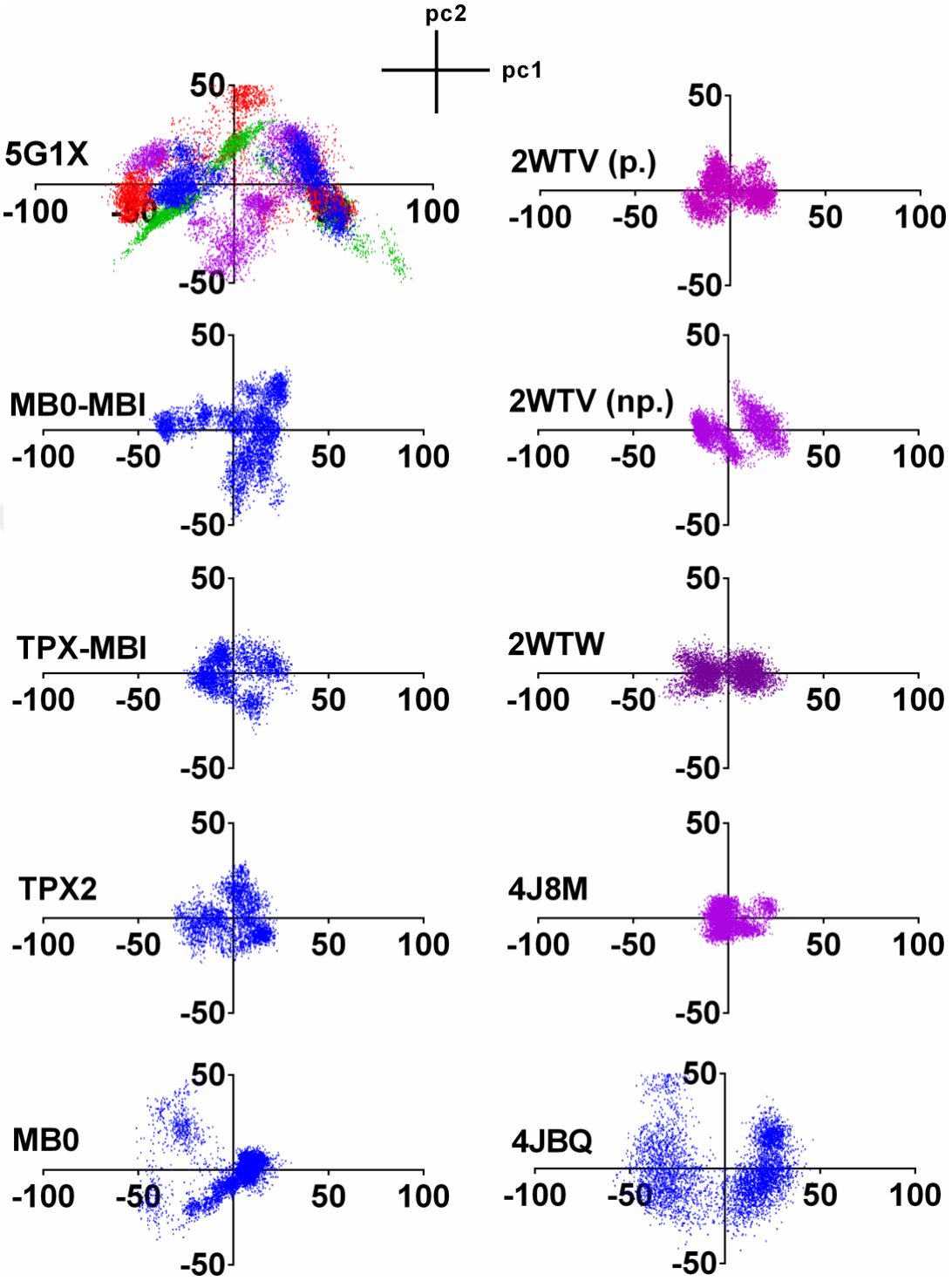

Figure 10. The representation of PCA loadings by plotting first two components of all complexes.

The first plot on the leftside of the panel are indicated replications of 5G1X. Each repetitions are colored blue (n=1), red (n=2), green (n=3) and purple (n=4), respectively. However, inhibitor bound complexes are colored by purple, protein partner complexes are colored by blue.

While the mobility distribution during the simulation in TPX2 resembles the fused structure (TPX2/MBI) in the form of the 90 degrees counterclockwise rotation, such similarity is not found between 5G1X MB0-I and MB0. Unlike partner-linked AurAs, inhibitor-bound AurA forms generate not only total scanning area in PC1-2 axes but also have more distinct and small clusters except 4JBQ. There are three tangled clusters seen at 2WTV, and its deviation is intensively dependent on PC1. The reduction of 2WTV, an unphosphorylated form, results in the regeneration of two discrete groupings from these embedded three pseudo-clusters. In 2WTW, it evokes the intermediate phase of the former structures with two clusters as unphosphorylated form and being PC1 dominated as a phosphorylated version of 2WTV.

On the other hand, according to the first two eigenvalues of 4J8M, total displacement throughout the simulation has almost always remained constant. Although a minor part of it disrupts the unity of that cluster, it might be assumed that there is a negligible deviation if all other structures are considered. When the residue-wise contribution of the first fifth PCA and RMSF results are examined, the activation loop and N-C terminals of 4J8M have as fluctuate as other inhibitor bound structures. The main reason for this less movable conformer plot of 4J8M might have originated from the computed 6 PCA nodes of 4J8M are very close to each other. Thus, while the first two PC data can explain more than 80% of all other structures, this value remains lower at 4J8M. Finally, in 4JBQ, two broad clusters are mirror images of each other. Although it does not exceed 50 in the positive and negative direction in PC1 and PC2, conformer mobility is varied on PC2. These two groups are similar to the blue repeat of 5G1X in terms of the number of clusters and their positions.

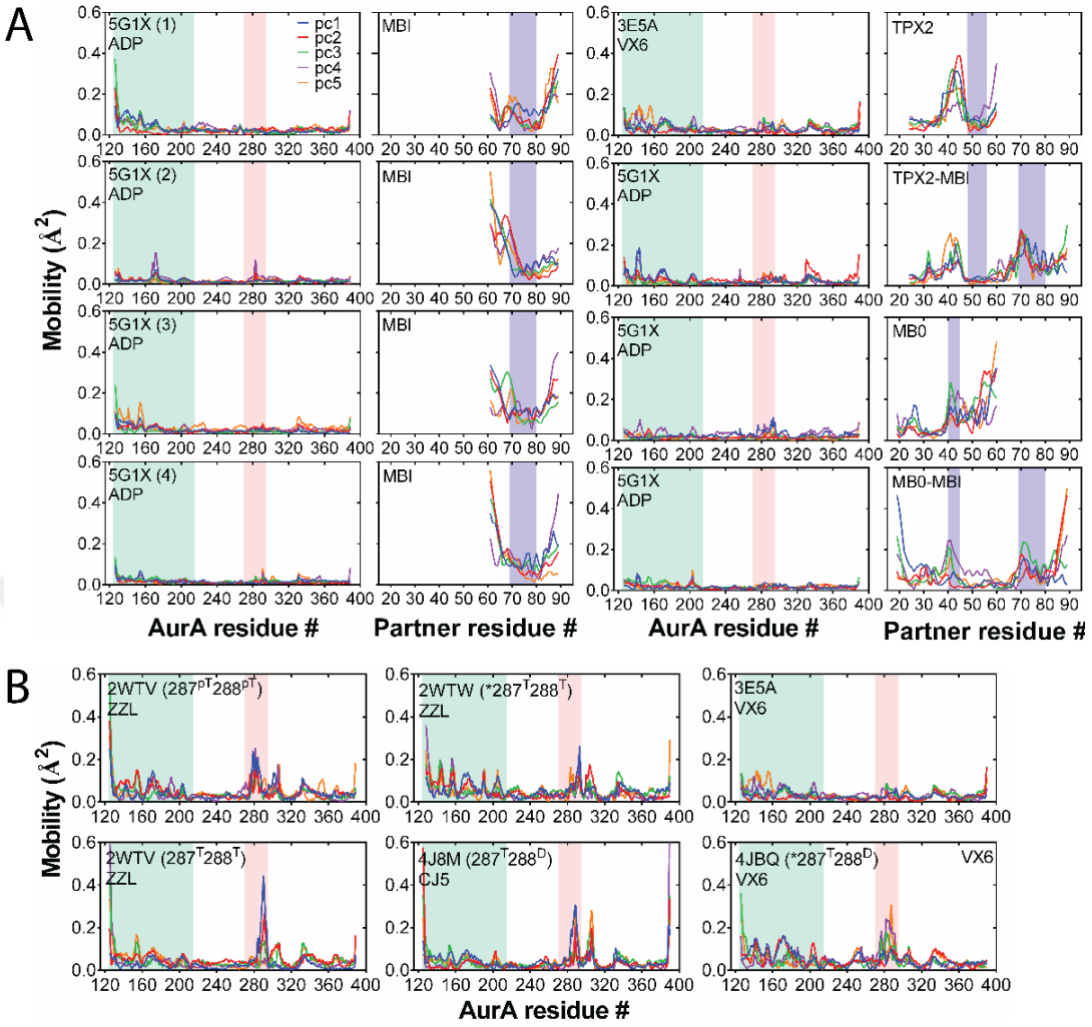

Figure 11. The residuewise contribution of PCA results by plotting first sixth components for both AurA and its protein partners.

We examined the atomic positional fluctuations of all structures captured in PC1 and PC2 dimensions. It would be more decisive to analyze the sectional differences of all the interconformers changes caused by ligands or proteins directly interacting with different regions of AurA. Therefore, the contributions of each amino acid to these displacements are computed in the scope of the first fifth PCs. The main difference between RMSF and reside-wise PCA assessment approach is that in the RMSF, it is based on the average of the distances in each frame in RMSD, while in PCA, it is utilized for statistically reduced variances.

The main difference between RMSF and residue-wise PCA computation is calculated according to the average distance in RMSD and RMSF, while in PCA, it is calculated individually for each statistically reduced variance after superimposing the protein concerning carbon alpha.

4.6 Distance Matrix Difference Between Initial and Final Step of the Simulations

In a distinct manner than PCA and RMSF, total displacements of AurA and its partners based on amino acids are examined during the simulation. In this way, we individually calculated the position matrices of each carbon alpha atom at the start and end of simulations of all systems with each other. The differences between these first and last frames of these carbon alphas will give information about the regions where the binding partners interact with the aurora. In Figure 9, the differences between the protein partners and AurA show depending on their positions at the start and end of the simulation. The fact that the Cα's of the protein binding complex have diverged from their initial state is indicated as dark blue, and their convergence is indicated as red lastly, the state where their total displacement is zero is indicated as white. In 4 repetitions of 5G1X, there is no apparent steady portion of N-Myc rather than other its elongated and fusion forms, which confirms the extreme mobility in our other analyzes. Plausibly, the N-Myc shifts dominantly from N-terminal to C-terminal of AurA, especially in third repeat N-Myc strictly interacting with AurA in between activation loop and at the end of the protein. The secondary structured part of N-Myc binds to AurA almost the same pattern in four systems. However, the most prominent intermolecular convergence occurred at the disordered N-terminal of N-Myc. All AurA/N-Myc interactions occur with the entire surface of the AurA except for the third repeat. The fluctuations in the N-terminus of AurA, which is seen as a result of the mobility in the third repeat PCA, might have originated from the extreme shifting of N-Myc on the structure. The considerable difference in the MBI/AurA interaction in

the elongated form and the 5G1X complex also occurred. In the extended form, there is a smooth approach to the entire surface of the AurA in the MB0 region of N-Myc and the interconnecting connection region (spanning from 48th to 60), while there is a convergence with AurA with only the N-terminal region of the MBI.

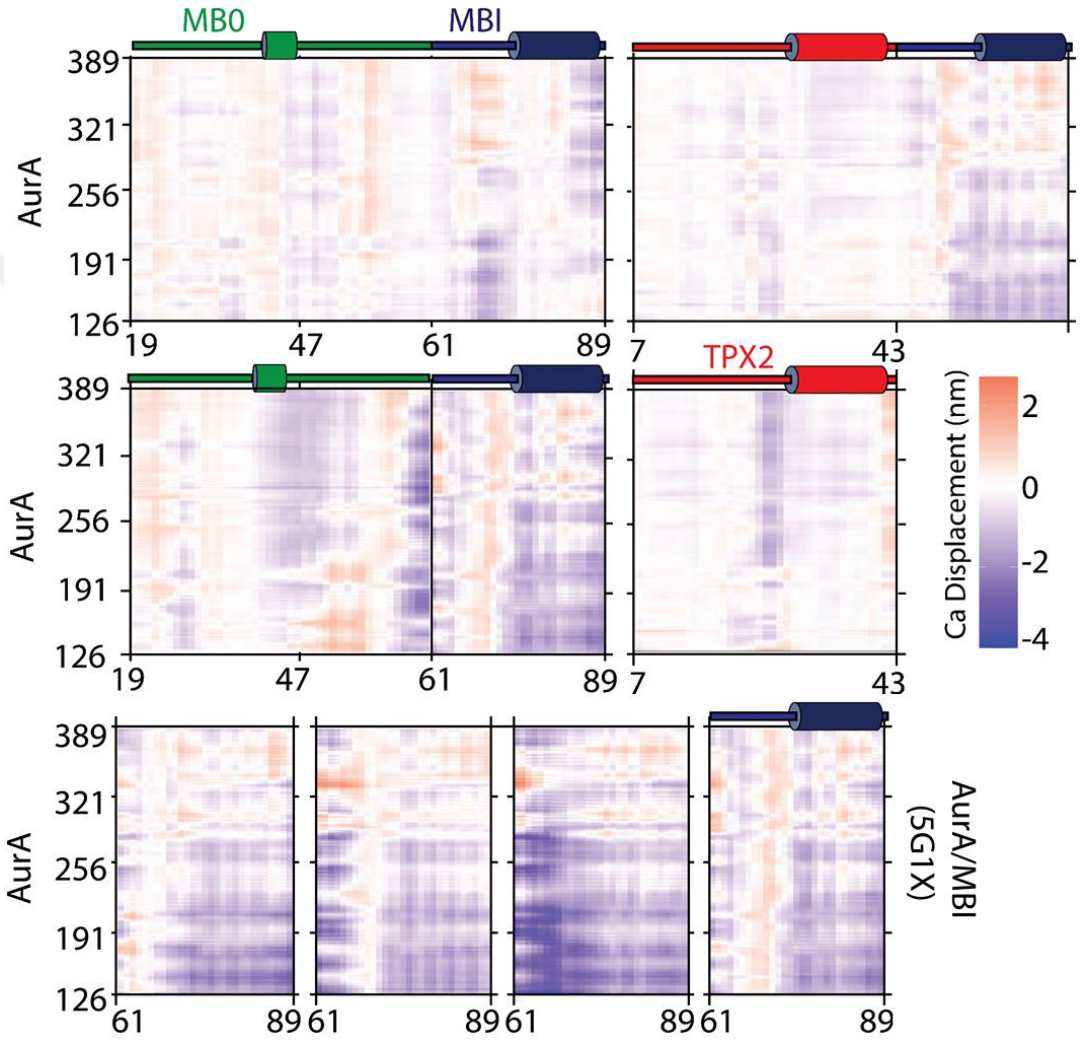

Figure 12. The distance matrix differences between Cα atoms of AurA and its protein partners.

On the upper side of each heatmaps, the locations of secondary motifs in protein partners are shown.

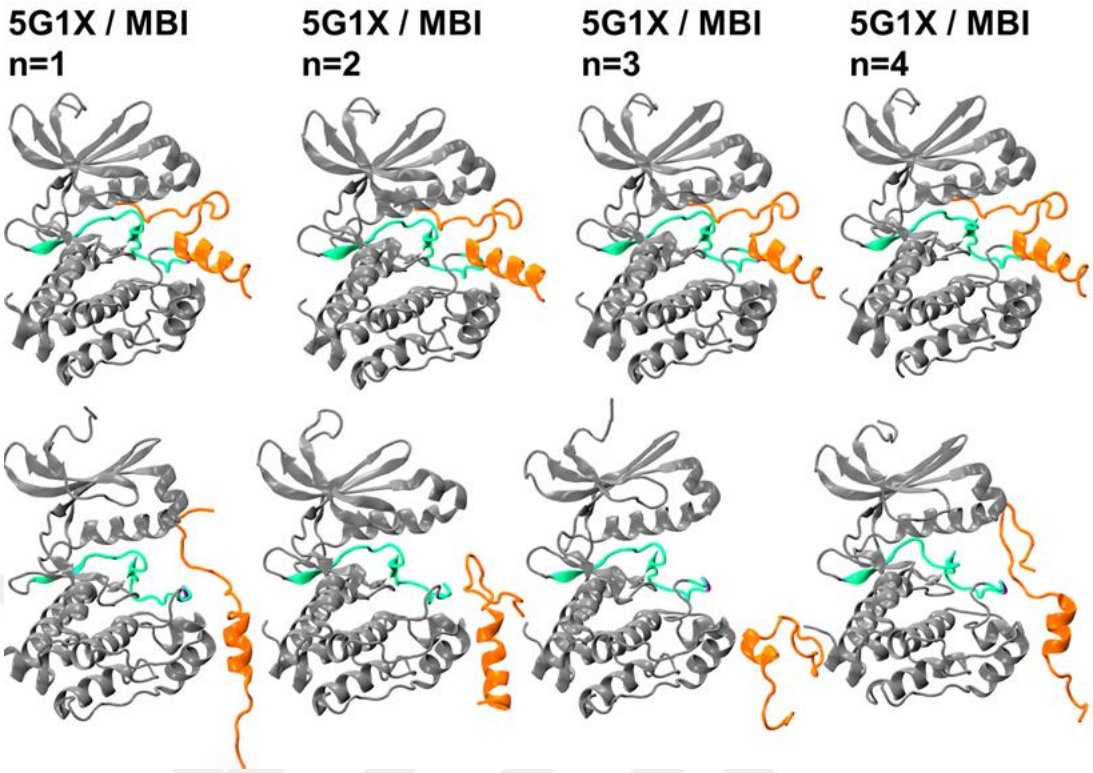

Figure 13. Structural differentiations of 5G1X repetitions from initial to final steps.

For all replications of 5G1X, AurA/-MB1 N-Myc stabilizations are conserved at the end of the MD simulations.

The C-terminal region of N-Myc moves away from the AurA. Similar to the AurA/MBI scenario, when only MB0 is bound to AurA, approximately the last five amino acids of MB0 are entirely dissociated from the complex. Otherwise, at the end of MB0, a distinct association dominantly towards the N-terminus of AurA, which has not ever been seen in the elongated version, is observed. In the 3E5A crystal, the region computationally constructed in TPX2 does not participate any interaction with AurA. Besides, the rest of them did not disturb the total displacement of TPX2.

Furthermore, this is the same portion of TPX2 as a rapid jump in the residue-wise contribution of PCA. In the computationally generated TPX2/MBI structure, the fluctuations at the same region have decreased, and the total distance difference of TPX2 has not changed. The N-Myc mobility in the fusion form is less than in the 5G1X crystal, even though the observed convergence in the secondary structure is still in a similar pattern at 5G1X (closing to the AurA). In the elongated form, MBI mobility is lower than both chimeric and solely MBI (5G1X). Especially in the beginning part of the helical portion of MBI has almost zero displacements. Consequently, MBI fluctuation is solved with the construction of the interacted part with the N-terminal of AurA.

4.7 Binding Free Energy Predictions of Protein Partners of AurA

Apart from these analyses, free binding energy assessment for each AurA protein partner complexes to compare binding affinities of each partner via using an amber scoring method. Like dynamical analysis results, the amber scores confirmed that only MBI could not provide enough for complex stabilization, calculated as -69.29 kcal/mol. Interestingly, the binding affinity of solely MB0 to AurA almost two times higher than 5G1X/MBI crystal which is reported as -135.99 kcal/mol. This result also proves that AurA favorably generates protein-protein interaction at the N-terminal lobe. However, only MB0 has a lower affinity as compared to TPX2 of the 3E5A complex, which is found as -159.71 kcal/mol. Related to distance matrix analysis, we showed that the addition of TPX2 to MBI performs joint stabilization in the chimeric form of the AurA complex. Besides this evidence, the free binding energy of TPX2/MBI form is recorded as -188.60 kcal/mol, which is the highest affinity to AurA in all 13 different structures.

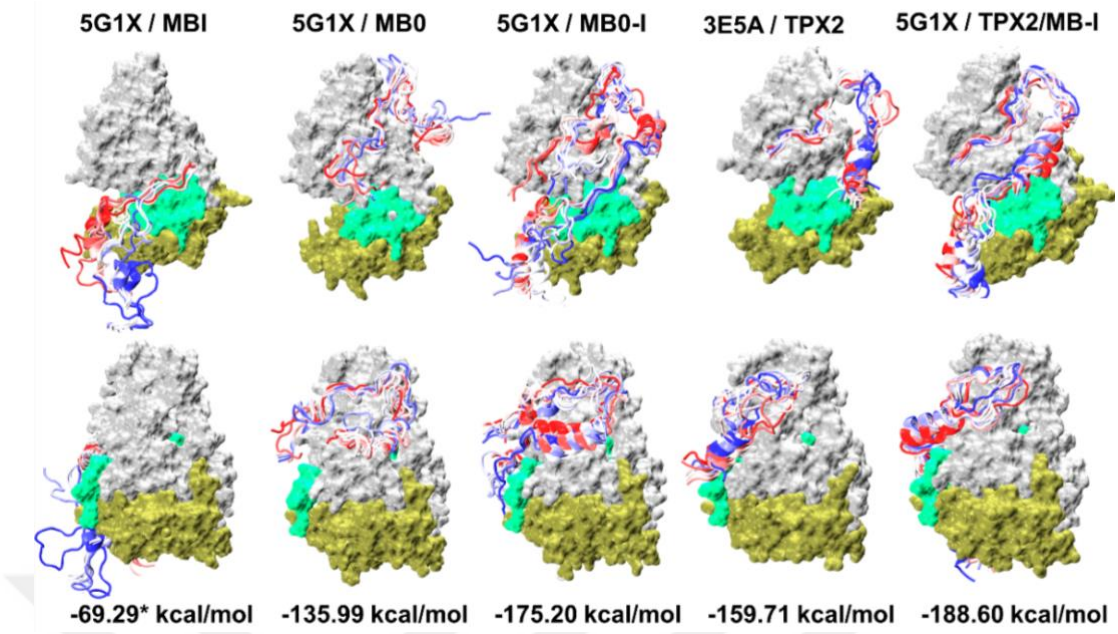

Figure 14. Binding free energy assessments of all AurA/protein complexes with structural models.

Both back and front side snapshots of the protein partners are demonstrated as top and bottom. AurAs are represented by surface and colored with silver (N-terminal), dark yellow (C-terminal) and light green (activation segment), respectively.

The opposite trend is observed in MB0-I / AurA and TPX2 / MBI / AurA complexes. Even if a decline is seen in the last frame, still the fused complex has the highest affinity in both classes. Since there is more binding energy in 5G1X MB0-I than MB0, this indicates that with the addition of MB0, MBI is also able to interact with AurA much more effectively. Even with this view, it can be interpreted that the MBI contribution in the stabilization of the complex in fused form is more than 5G1X MB0-I. In conclusion, AurA N-terminal stabilization plays a key role in mimicking N-Myc for peptide design.

5. DISCUSSION AND CONCLUSION

To investigate the structural mechanism through protein binding of AurA complexes, we analyzed eight different AurA to inhibit the N-Myc protein, which prevents its degradation due to stably unrevealed affinity toward AurA. Here, we ascertained all the structural similarities and differences of the complexes in binding with TPX2 and N-Myc on the surface of AurA via computational perspective. On the other hand, it has also been investigated whether AurA targets small molecular inhibitors, which are currently undergoing phase studies and have already proven to have a negative impact on the catalytical activity of AurA.

For this purpose, both the conformation, which is known as having an active form and the changed conformation caused by binding inhibitors are also examined. As a result of the examination of 173 of AurA proteins basically, two distinct conformations are observed in this protein in the PDB. Therefore, the region that can only prevent the binding of the protein partner of AurA has been determined as the activation segment in all these structures. Due to the fact that the VX6 bound, TPX2/AurA complex (3E5A) remained stable throughout the simulation, and whose AurA protein preserves in both the catalytic and active state. Additionally, the same structure has the highest affinity after the constructed structures in protein-protein interaction calculations. Apart from VX6, in AurA structures that change the active loop, like 4J8M and 2WTV, the mobility of these structures comes into prominence instead of other domains in both RMSD and RMSF results during 500 ns simulations.

Similar to the MD studies, in 2WTW, which is referred another snapshot of the same structure, the activation loop is reported as lost due to this mobility. This missing

part is re-constructed by the homology modeling method. As a result, this remodeled region is similar in the structure due to AurA of VX6 (4JBQ). With the presence of this structure, the activation ring of the inhibitor-bound AurA complexes might not be found stably in different conformations. Therefore, in this study, it is revealed that known AurA inhibitors could not primarily inhibit protein-protein binding.

Besides the conformational change in the activation segment, these inhibitors have an allosteric effect on the catalytic motives in the core region of AurA. Particularly HRD and DFG motifs, which act as an essential role in kinases. Both the interactions between them and other brutal motifs of AurA are decreased in comparison to the active form (compared to 5G1X variations). On the other hand, the distances between these motifs are examined because elevated distance increment between these motifs is catalytically incompatible in such kinases (3). While 2WTV lost their interactions in both forms and 4JBQ, the inhibitor-bound 4J8M and 2WTW are able to keep this distance stably. The interaction between these motifs could not provide any evidence either by inhibitor binding or by loop rotation. From this point of view, the region where these changes occur in AurA with the binding of inhibitors is not directly related to the interaction with binding partners. As shown in the essential dynamics and trajectory analysis, AurA prefers the N-terminal domain in protein-protein interactions.

The hydrophobic spine in the core region of AurA, which also contains some amino acids in these motifs, is among the regions frequently targeted by small molecule inhibitors targeting AurA. Preservation of this hydrophobic backbone in the serine-threonine kinase protein family is also an essential factor for the self-stabilization of the kinases like AurA. This spin is formed by aligning four amino acids which are Gln185, Leu196, His254, and Phe275, respectively. In all structures, RMSF results of both His254 and Phe275, which have higher molecular weight, have higher

mobility than in the Gln185 and Leu196. Generally, although the fluctuations of inhibitor-bound AurA structures are intensively found rather than protein-partners complexes, the exception is also seen in 5G1X/MB0, especially in His254. Similarly, in the other kinase activity assessment studies, it is not possible to distinguish which in the hydrophobic spine dynamics directly affects the AurA inhibitors on the activation loop. Because the residual elevation is experienced in both forms of AurA crystals. On the other hand, we have also obtained a different finding that although 4J8M of Phe275 has the highest CHI angle displacement, this situation did not significantly affect the hydrophobic spin conformation that proves the rotation in the CHI1 angle may not directly affect the hydrophobic spin, even if the activation loop is in an inactive form. In the protein-partner bound AurA structures, all spins preserved their existence during their simulation. As a result, Leu 196 and Gln185 residues of this unique pocket may influence protein binding to AurA due to their location. However, in the RMSF study, the results of this spin, especially Leu196, maintains its stagnation in all cases regardless of inhibitor type and activation conformations.

Besides these known motif interactions, another evidence is associated with Serine-Threonine kinases activity like AurA, the salt bridge established between positions Glu181 - Lys162. This unique interaction depends on the distance results similar to the DFG-HRD motif studies that mean the evolutionary specialized interaction is preserved in the whole activation segment in an active form, regardless of whether the inhibitor is bound, except for the 4JBQ. Because in the 4JBQ complex, in the binding of solely VX6 to AurA, Glu181 is blocked by the rotation of the side chain. However, it is regained with the interaction of TPX2 (3E5A). In VX6, independent of the loop conformation state, this static interaction is still prevented; these charged residues are come to appropriate conditions to make a stable interaction in the AurA complex by connecting TPX2. This salt bridge is not only dependent on protein interactions with the N-terminal lobe of AurA, but stable salt bridge interactions have also been seen in all protein partner interactions, at least for more than half of the simulations.

Effect of kinase activity on protein-protein interaction (HRD and DFG motif, hydrophobic spine, salt bridge) none of them distinctly separate their AurA conformation. Also, none of the currently available inhibitors can create a destabilization in AurA that would directly prevent the binding of its protein partners. Because they are not designed to directly block this interaction, enzymatically inactivity may prevent neither N-Myc nor TPX2 from binding. Therefore, it is aimed to prevent this binding with a peptide design that will mimic N-Myc.

In 5G1X, the MB1 highly fluctuates, so different replicas are performed, but in any case, there is much activity partially dissociated from the AurA and N and C terminals of the AurA (Figure 10). In its extended version, this problem disappeared; even the MB0 state showed similar characteristics to the stabilizer partner is TPX2. This situation showed that AurA preferably performs protein-protein interaction with N-terminal dominantly. Therefore, the interactions at this terminal lobe of AurA play a much more vital role in a design that will have a forceful affinity to AurA and prevent it from binding by mimicking N-Myc. The extreme fluctuations in MBI decreased to minimal by constructing both chimeric form and missing portion, and the mobility in N and C terminal of AurA decreased to normal levels.

Essential dynamics and trajectory analysis give a piece of information about the complex mobility during the simulation. Therefore, to demonstrate all these fluctuations, the distance matrix differences between the first and last frames of all studied AurA complexes. With this study, heatmaps are created to visualize the distances of each residue of AurA's affiliated protein partner to each other. In the case of stably binding between protein partners and AurA, it is assumed to be preserved from the beginning to the end of the simulation. The mobility in both directions (positively or negatively) is examined as undesirable for the overall structure. The main reason for the assumption is that we do not consider the distance between the

atoms at the beginning and the ending. For example, when a residue with an initial distance between some parts of AurA is 40 Å, and it would be calculated as 38 Å at the end of the simulation, the total displacement of this atom appears to stabilize the overall complex. However, this convergence does not actually play a role in any secondary interaction. As a result, in cases where the difference between these frames is minimal, it is more accurately concluded that a favorable intermolecular interaction should be established. The best-fitted interaction to this trend is TPX2/AurA in all complexes. Compared to the derived structures of MBI within the partner proteins, which are 5G1X (MBI), 5G1X (MB0-I), and 5G1X (TPX2/MBI), in fusion form of MBI has the lowest residual displacement. Likely, the comparison of these partners focused solely on MB0 of 5G1X and 3E5A complexes depending on the N-terminal lobe stabilization of the AurA, TPX2 has still better results. Remarkably, there are no residues whose total displacement to AurA does not change at all in the presence of MBI alone. On the other hand, the binding of TPX2 to MBI not only positively affected the total mobility in MBI but also brought its displacement closer to zero when compared to the form in which is a single form of TPX2 (3E5A). With this chimeric structure, a bidirectional improvement has been achieved in protein-partner interaction. It has an important role in designing the peptide, which is planned to be developed because it reduces both the high mobility in MBI and its contribution to the binding of TPX2.

To support these findings, free energy binding assessment analysis has been performed on both the structures constructed and the crystal structures already present. As a result of the analysis, it is seen that the general structure is not sufficient for stabilization only in the presence of MBI. With the remodeling of MB0 to the one reported as missing in the crystal, the affinity of the N-Myc protein to bind to AurA increased pretty high. With the modeling of MB0, extreme mobility in MBI has also decreased. In this way, it started to contribute to the complex stabilization in MBI. As it is known that all N-Myc regions exist in cancer types in which N-Myc is amplified under normal conditions, N-Myc AurA affinity is quite elevated. On the other hand,

as the advanced stage of our study, the binding affinity of TPX2, known as the stabilizer partner of AurA, binds to the MB0 region of AurA to create a peptide design that will compete with N-Myc is also examined. As a result, the highest binding affinity in all crystal and constructed structures is obtained with the chimeric TPX2 / MBI protein created to see the effect of MBI on AurA interaction, as well as the affinity of TPX2 to AurA. In our peptide study planned for N-Myc inhibition targeting AurA, examining the critical interactions of TPX2 with AurA and detailed examination of the intermolecular interactions between MB0 will provide a very insightful perspective.

In this thesis, we investigated the structural mechanism behind protein-protein interaction and small molecule interaction with AurA by enhancing inhibiting approach for AurA/N-Myc interaction. Besides, N-Myc is prevented from its proteasomal degradation in neuroblastoma via interacting with AurA. In the case of N-Myc level is amplified due to these interactions arising only from intermolecular affinity that is not found in any pathway with AurA. Like other transcription factors, N-Myc is classified as undruggable which cannot be targeted directly. In this study, we first revealed whether small chemical inhibitors that inhibit AurA cause an allosteric change in the binding site of N-Myc using structural biology methods. Thus, the key motifs and unique interactions for the catalytic activity of AurA are examined. A clear distinction between the phosphorylation state and the variation of rotation in the activation and the interactions associated with this catalytically active loop in the inhibitor-bound crystals could not be found. Since these already known inhibitors are not directly in the binding site of N-Myc in AurA, it is understandable that they cannot inhibit this interaction. Although each ligand inhibits different types of interactions, this type of destabilization has also been seen in protein-bound complexes in some cases. A stable complex stabilization could not be observed as a result of 4 repetitions in the 5G1X (MBI) complex, which is only the crystal and backbone of our study. Later, with the addition of the missing portion of the MB motif with homology modeling, we concluded that the interaction of MB0 on the AurA surface allows the MBI to be stably bonded. It also confirms our hypothesis in the other structure constructed, 5G1X (TPX2/MBI) and crystallized AurA/TPX2 (3E5A) complex.

Consequently, investigating the structural mechanism of AurA, which is predicted via comparative modeling algorithms, reveals that the missing portion of the crystal structure might have essential for the complex stabilization. Although it is thought to have no significant role in overall stabilization, since it is modeled structures reported as loss in crystallization studies due to the mobility in the complex, with the re-modeling of MB0 reported as missing in PDB, provided vital importance on the complex against all dynamical analysis. Structural biology studies have enabled such problems to be recreated with computational methods.

Future study would be quite insightful to examine all protein-protein of the interaction of N-terminal lobe of AurA at a residue-specific level to achieve N-Myc inhibition, targeting AurA. Thus, with the designing of a novel peptide, we are planning to provide the protein partner inhibition of AurA and eliminate the stabilization of AurA such as TPX2 and maintain the N-Myc degradation at the same time.

6. APPENDICES

Appendix 1. Table of all AurA complexes in PDB

To observe the dynamical similarities of AurA proteins, 173 AurA crystal structures are extracted in PDB. The crystals pool is involved in their characteristics consisting of ligand name, ligand formula (SMILES code), source organism, sequence, the molecular weight of both ligands and proteins, and chain length.

PDB ID	Loop Conformation	Chain Length	Source Organism	Molecular Weight (Entity)	Ligand ID	Ligand MW (g/mol)
1MQ4	active	272	Homo sapiens	31.44	MG	24.305
1MUO	missing	297	Homo sapiens	34.432	ADN	267.241
1OL5	active	282	Homo sapiens	32.849	ADP	427.201
1OL6	missing	282	Homo sapiens	32.688	ATP	507.181
1OL7	active	282	Homo sapiens	32.849	ADP	427.201
2BMC	missing	306	Homo sapiens	35.305	MPY	497.591
2C6D	missing	275	Homo sapiens	31.985	GOL	92.094
2C6E	missing	283	Homo sapiens	32.773	HPM	529.59
2DWB	missing	285	Homo sapiens	33.203	SO4	96.063
2J4Z	inactive	306	Homo sapiens	35.277	626	448.541
2J50	missing	280	Homo sapiens	32.369	627	474.555
2NP8	missing	272	Homo sapiens	31.44	SO4	96.063
2W1C	active	275	Homo sapiens	32.318	L0C	421.447
2W1D	missing	275	Homo sapiens	32.158	L0D	184.197
2W1E	missing	275	Homo sapiens	32.158	L0E	418.472
2W1F	missing	275	Homo sapiens	32.158	L0F	303.318

Appendix 1. Table of all AurA complexes in PDB (cont.)

2WQE	**missing**	**262**	**Homo sapiens**	**30.507**	**ADP**	**427.201**
2WTV	**inactive**	**285**	**Homo sapiens**	**33.229**	**ZZL**	**476.862**
2WTW	**missing**	**285**	**Homo sapiens**	**32.993**	**ZZL**	**476.862**
2X6D	**active**	**285**	**Homo sapiens**	**32.949**	**SO4**	**96.063**
2X6E	**missing**	**285**	**Homo sapiens**	**32.949**	**YM4**	**551.481**
2X81	**missing**	**272**	**Homo sapiens**	**31.44**	**ZZL**	**476.862**
2XNE	**missing**	**272**	**Homo sapiens**	**31.626**	**ASH**	**406.868**
2XNG	**missing**	**283**	**Homo sapiens**	**32.821**	**A0H**	**513.012**
2XRU	**missing**	**280**	**Homo sapiens**	**32.397**	**400**	**502.631**
3COH	**missing**	**268**	**Homo sapiens**	**31.008**	**83H**	**348.441**
3D14	**missing**	**272**	**Mus musculus**	**31.549**	**AK1**	**464.487**
3D15	**missing**	**272**	**Mus musculus**	**31.549**	**AK2**	**430.934**
3D2I	**missing**	**272**	**Mus musculus**	**31.549**	**AK3**	**462.451**
3D2K	**missing**	**272**	**Mus musculus**	**31.549**	**AK4**	**472.908**
3DAJ	**missing**	**272**	**Mus musculus**	**31.563**	**FXG**	**423.511**
3DJ5	**missing**	**272**	**Mus musculus**	**31.549**	**AK5**	**502.384**
3DJ6	**missing**	**272**	**Mus musculus**	**31.549**	**AK6**	**460.548**
3DJ7	**missing**	**272**	**Mus musculus**	**31.549**	**AK7**	**502.312**
3E5A	**active**	**268**	**Homo sapiens**	**31.174**	**VX6**	**464.586**
3EFW	**missing**	**267**	**Homo sapiens**	**31.037**	**AK8**	**494.468**
3FDN	**missing**	**279**	**Homo sapiens**	**32.359**	**MMH**	**406.438**
3H0Y	**missing**	**268**	**Homo sapiens**	**31.048**	**48B**	**449.865**
3H0Z	**missing**	**268**	**Homo sapiens**	**31.048**	**45B**	**602.058**
3H10	**inactive**	**268**	**Homo sapiens**	**31.048**	**97B**	**559.009**
3HA6	**active**	**268**	**Homo sapiens**	**31.254**	**2JZ**	**511.55**
3K5U	**missing**	**279**	**Homo sapiens**	**32.359**	**PFQ**	**331.368**
3LAU	**missing**	**287**	**Homo sapiens**	**33.342**	**OFI**	**295.336**
3M11	**missing**	**279**	**Homo sapiens**	**32.359**	**AKI**	**525.6**
3MYG	**missing**	**272**	**Homo sapiens**	**31.44**	**PG4**	**194.226**
3NRM	**active**	**283**	**Homo sapiens**	**32.558**	**NRM**	**297.338**
3O50	**missing**	**267**	**Homo sapiens**	**31.037**	**LJE**	**450.413**

Appendix 1. Table of all AurA complexes in PDB (cont.)

3O51	**missing**	**267**	**Homo sapiens**	**31.037**	**LJF**	**504.514**
3P9J	**missing**	**268**	**Homo sapiens**	**31.048**	**P9J**	**317.345**
3QBN	**missing**	**281**	**Homo sapiens**	**32.502**	**E9Z**	**334.801**
3R21	**missing**	**271**	**Homo sapiens**	**31.347**	**D36**	**444.554**
3R22	**missing**	**271**	**Homo sapiens**	**31.347**	**D37**	**401.486**
3UNZ	**inactive**	**279**	**Homo sapiens**	**32.359**	**0BZ**	**324.309**
3UO4	**active**	**279**	**Homo sapiens**	**32.359**	**0C0**	**382.415**
3UO5	**active**	**279**	**Homo sapiens**	**32.359**	**0BX**	**306.319**
3UO6	**inactive**	**279**	**Homo sapiens**	**32.359**	**0BY**	**340.764**
3UOD	**active**	**279**	**Homo sapiens**	**32.359**	**0C3**	**374.317**
3UOH	**inactive**	**279**	**Homo sapiens**	**32.359**	**0C4**	**385.215**
3UOJ	**inactive**	**279**	**Homo sapiens**	**32.359**	**0C5**	**331.328**
3UOK	**inactive**	**279**	**Homo sapiens**	**32.359**	**0C6**	**358.754**
3UOL	**inactive**	**279**	**Homo sapiens**	**32.359**	**0C7**	**364.792**
3UP2	**active**	**279**	**Homo sapiens**	**32.359**	**0C8**	**390.316**
3UP7	**active**	**279**	**Homo sapiens**	**32.359**	**0C9**	**350.328**
3VAP	**missing**	**272**	**Homo sapiens**	**31.44**	**0FY**	**563.673**
3W10	**inactive**	**278**	**Homo sapiens**	**32.155**	**RO9**	**330.383**
3W16	**missing**	**278**	**Homo sapiens**	**32.215**	**P9J**	**317.345**
3W18	**missing**	**278**	**Homo sapiens**	**32.215**	**N13**	**451.455**
3W2C	**missing**	**261**	**Homo sapiens**	**30.309**	**N15**	**427.502**
4B0G	**missing**	**283**	**Homo sapiens**	**32.821**	**VEK**	**457.327**
4BN1	**active**	**285**	**Homo sapiens**	**33.141**	**ADP**	**427.201**
4BYI	**missing**	**285**	**Homo sapiens**	**32.949**	**FH3**	**387.867**
4BYJ	**missing**	**285**	**Homo sapiens**	**32.949**	**FH5**	**373.84**
4C3P	**missing**	**282**	**Homo sapiens**	**32.689**	**ACP**	**505.208**
4C3R	**missing**	**282**	**Homo sapiens**	**32.689**	**ACP**	**505.208**
4CEG	**active**	**285**	**Homo sapiens**	**32.965**	**ADP**	**427.201**
4DEA	**active**	**279**	**Homo sapiens**	**32.359**	**EDO**	**62.068**
4DEB	**active**	**279**	**Homo sapiens**	**32.359**	**NHJ**	**373.332**
4DED	**active**	**279**	**Homo sapiens**	**32.359**	**NHU**	**348.359**

Appendix 1. Table of all AurA complexes in PDB (cont.)

4DEE	**active**	**279**	**Homo sapiens**	**32.359**	**MG**	**24.305**
4DHF	**missing**	**271**	**Homo sapiens**	**31.347**	**0K6**	**450.537**
4J8M	**inactive**	**279**	**Homo sapiens**	**32.479**	**CJ5**	**522.525**
4J8N	**active**	**279**	**Homo sapiens**	**32.359**		
4JAI	**missing**	**284**	**Homo sapiens**	**33.045**	**XU2**	**406.436**
4JAJ	**active**	**284**	**Homo sapiens**	**33.045**	**XU1**	**196.205**
4JBO	**active**	**279**	**Homo sapiens**	**32.359**	**WPH**	**536.624**
4JBP	**missing**	**279**	**Homo sapiens**	**32.359**	**YPH**	**592.687**
4JBQ	**missing**	**279**	**Homo sapiens**	**32.359**	**VX6**	**464.586**
4O0S	**missing**	**282**	**Homo sapiens**	**32.689**	**ADN**	**267.241**
4O0U	**missing**	**282**	**Homo sapiens**	**32.709**	**ADN**	**267.241**
4O0W	**missing**	**282**	**Homo sapiens**	**32.714**	**ADN**	**267.241**
4PRJ	**missing**	**269**	**Homo sapiens**	**31.139**	**2VU**	**408.415**
4UYN	**missing**	**287**	**Homo sapiens**	**33.342**	**Y3M**	**474.532**
4UZD	**missing**	**287**	**Homo sapiens**	**33.328**	**QMN**	**468.504**
4UZH	**missing**	**287**	**Homo sapiens**	**33.342**	**JVE**	**284.288**
4ZS0	**missing**	**285**	**Homo sapiens**	**32.949**	**4QV**	**266.255**
4ZTQ	**missing**	**285**	**Homo sapiens**	**32.949**	**4RM**	**367.465**
4ZTR	**missing**	**285**	**Homo sapiens**	**32.949**	**4RJ**	**459.52**
4ZTS	**missing**	**285**	**Homo sapiens**	**32.949**	**4RK**	**482.56**
5AAD	**missing**	**285**	**Homo sapiens**	**32.885**	**5GX**	**403.868**
5AAE	**missing**	**285**	**Homo sapiens**	**32.885**	**7HD**	**408.844**
5AAF	**missing**	**285**	**Homo sapiens**	**32.885**	**NL4**	**474.945**
5AAG	**missing**	**285**	**Homo sapiens**	**32.885**	**6F2**	**530.024**
5DN3	**active**	**272**	**Homo sapiens**	**31.536**	**MG**	**24.305**
5DNR	**active**	**272**	**Homo sapiens**	**31.536**	**MG**	**24.305**
5DOS	**missing**	**273**	**Homo sapiens**	**31.808**	**MG**	**24.305**
5DPV	**missing**	**273**	**Homo sapiens**	**31.808**	**5DN**	**346.151**
5DR2	**active**	**273**	**Homo sapiens**	**31.808**	**50**	**328.16**
5DR6	**missing**	**273**	**Homo sapiens**	**31.808**	**50**	**328.16**
5DR9	**missing**	**273**	**Homo sapiens**	**31.808**	**SKE**	**394.356**

Appendix 1. Table of all AurA complexes in PDB (cont.)

5DRD	**missing**	**273**	**Homo sapiens**	**31.808**	**MG**	**24.305**
5DT0	**missing**	**273**	**Homo sapiens**	**31.808**	**SKE**	**394.356**
5DT3	**active**	**273**	**Homo sapiens**	**31.918**	**MG**	**24.305**
5DT4	**active**	**273**	**Homo sapiens**	**31.838**	**MG**	**24.305**
5EW9	**missing**	**271**	**Homo sapiens**	**31.537**	**5VC**	**461.937**
5G15	**active**	**282**	**Homo sapiens**	**32.689**	**ACP**	**505.208**
5G1X	**active**	**285**	**Homo sapiens**	**32.965**	**ADP**	**427.201**
5L8J	**missing**	**285**	**Homo sapiens**	**32.965**	**ADP**	**427.201**
5L8K	**active**	**285**	**Homo sapiens**	**32.965**	**ADP**	**427.201**
5L8L	**active**	**285**	**Homo sapiens**	**32.965**	**ADP**	**427.201**
5LXM	**active**	**283**	**Homo sapiens**	**32.837**	**ADP**	**427.201**
5OBJ	**missing**	**272**	**Homo sapiens**	**31.456**	**MG**	**24.305**
5OBR	**missing**	**272**	**Homo sapiens**	**31.456**	**9QT**	**301.7**
5ODT	**missing**	**283**	**Homo sapiens**	**32.756**	**ADP**	**427.201**
5ONE	**missing**	**285**	**Homo sapiens**	**32.949**	**9YQ**	**535.596**
5ORL	**active**	**265**	**Homo sapiens**	**30.798**	**ADP**	**427.201**
5ORN	**active**	**265**	**Homo sapiens**	**30.798**	**ADP**	**427.201**
5ORO	**active**	**265**	**Homo sapiens**	**30.798**	**ADP**	**427.201**
5ORP	**active**	**265**	**Homo sapiens**	**30.798**	**ADP**	**427.201**
5ORR	**active**	**265**	**Homo sapiens**	**30.798**	**ADP**	**427.201**
5ORS	**active**	**265**	**Homo sapiens**	**30.798**	**ADP**	**427.201**
5ORT	**active**	**265**	**Homo sapiens**	**30.798**	**ADP**	**427.201**
5ORV	**active**	**265**	**Homo sapiens**	**30.798**	**ADP**	**427.201**
5ORW	**active**	**265**	**Homo sapiens**	**30.798**	**ADP**	**427.201**
5ORX	**active**	**265**	**Homo sapiens**	**30.798**	**ADP**	**427.201**
5ORY	**active**	**265**	**Homo sapiens**	**30.798**	**ADP**	**427.201**
5ORZ	**active**	**265**	**Homo sapiens**	**30.798**	**ADP**	**427.201**
5OS0	**active**	**265**	**Homo sapiens**	**30.798**	**ADP**	**427.201**
5OS1	**active**	**265**	**Homo sapiens**	**30.798**	**ADP**	**427.201**
5OS2	**missing**	**265**	**Homo sapiens**	**30.718**	**ADP**	**427.201**
5OS3	**active**	**265**	**Homo sapiens**	**30.798**	**ADP**	**427.201**

Appendix 1. Table of all AurA complexes in PDB (cont.)

5OS4	**active**	**265**	**Homo sapiens**	**30.798**	**ADP**	**427.201**
5OS5	**active**	**268**	**Homo sapiens**	**31.199**	**ADP**	**427.201**
5OS6	**active**	**265**	**Homo sapiens**	**30.798**	**ADP**	**427.201**
5OSD	**active**	**267**	**Homo sapiens**	**31.085**	**ADP**	**427.201**
5OSE	**active**	**265**	**Homo sapiens**	**30.798**	**ADP**	**427.201**
5OSF	**active**	**265**	**Homo sapiens**	**30.798**	**ADP**	**427.201**
5ZAN	**missing**	**281**	**Homo sapiens**	**32.56**	**9A6**	**425.529**
6C2R	**missing**	**272**	**Homo sapiens**	**31.44**	**SO4**	**96.063**
6C2T	**missing**	**272**	**Homo sapiens**	**31.44**	**EGJ**	**525.037**
6C83	**missing**	**285**	**Homo sapiens**	**32.991**	**ACP**	**505.208**
6CPE	**missing**	**285**	**Homo sapiens**	**32.991**	**P4G**	**162.227**
6CPF	**missing**	**285**	**Homo sapiens**	**32.991**	**ACP**	**505.208**
6CPG	**missing**	**285**	**Homo sapiens**	**32.991**	**35R**	**381.432**
6GRA	**missing**	**285**	**Homo sapiens**	**32.949**	**F8Z**	**590.667**
6HJJ	**missing**	**285**	**Homo sapiens**	**32.875**	**G7T**	**528.501**
6HJK	**missing**	**285**	**Homo sapiens**	**32.875**	**G7W**	**512.459**
6I2U	**active**	**285**	**Homo sapiens**	**33.109**	**COA**	**767.534**
6R49	**missing**	**285**	**Homo sapiens**	**32.965**	**ADP**	**427.201**
6R4A	**active**	**285**	**Homo sapiens**	**32.965**	**ADP**	**427.201**
6R4B	**active**	**285**	**Homo sapiens**	**32.965**	**ADP**	**427.201**
6R4C	**active**	**285**	**Homo sapiens**	**32.965**	**ADP**	**427.201**
6R4D	**active**	**285**	**Homo sapiens**	**32.965**	**ADP**	**427.201**
6VPG	**active**	**292**	**Homo sapiens**	**34.067**	**ANP**	**506.196**
6VPH	**inactive**	**292**	**Homo sapiens**	**34.275**	**CL**	**35.453**
6VPI	**inactive**	**292**	**Homo sapiens**	**33.898**	**ANP**	**506.196**
6VPJ	**missing**	**292**	**Homo sapiens**	**33.899**	**ANP**	**506.196**
6VPL	**missing**	**292**	**Homo sapiens**	**33.987**	**MG**	**24.305**
6VPM	**missing**	**292**	**Homo sapiens**	**33.987**	**MG**	**24.305**
6XKA	**missing**	**292**	**Homo sapiens**	**33.907**	**COA**	**767.534**
6Z4Y	**missing**	**285**	**Homo sapiens**	**32.949**	**CIT**	**192.124**
7AYH	**missing**	**285**	**Homo sapiens**	**32.949**	**S9H**	**360.409**

Appendix 1. Table of all AurA complexes in PDB (cont.)

7AYI	**missing**	**285**	**Homo sapiens**	**32.949**	**S9K**	**330.383**

7. REFERENCES

1. Roskoski R. Classification of small molecule protein kinase inhibitors based upon the structures of their drug-enzyme complexes. Pharmacol Res [Internet]. 2016;103:26–48. Available from: http://dx.doi.org/10.1016/j.phrs.2015.10.021

2. Roskoski R. A historical overview of protein kinases and their targeted small molecule inhibitors. Pharmacol Res [Internet]. 2015 Oct;100:1–23. Available from: http://dx.doi.org/10.1016/j.phrs.2015.07.010

3. Bayliss R, Fry A, Haq T, Yeoh S. On the molecular mechanisms of mitotic kinase activation. Open Biol [Internet]. 2012 Nov;2(11):120136. Available from: https://royalsocietypublishing.org/doi/10.1098/rsob.120136

4. Kivinummi K, Urbanucci A, Leinonen K, Tammela TLJ, Annala M, Isaacs WB, et al. The expression of AURKA is androgen regulated in castration-resistant prostate cancer. Sci Rep. 2017 Dec 1;7(1).

5. Dodson CA, Kosmopoulou M, Richards MW, Atrash B, Bavetsias V, Blagg J, et al. Crystal structure of an Aurora-A mutant that mimics Aurora-B bound to MLN8054: Insights into selectivity and drug design. Biochem J. 2010;427(1):19–28.

6. Tang et al. 2005, Kelsey C. Martin Mhatre V. Ho J-AL. 基因的改变NIH Public Access. Bone [Internet]. 2012;23(1):1–7. Available from: https://www.ncbi.nlm.nih.gov/pmc/articles/PMC3624763/pdf/nihms412728.pdf

7. Wu JM, Chen CT, Coumar MS, Lin WH, Chen ZJ, Hsu JTA, et al. Aurora kinase inhibitors reveal mechanisms of HURP in nucleation of centrosomal and kinetochore microtubules. Proc Natl Acad Sci U S A. 2013;110(19):1779–87.

8. Ding L, Gu H, Gao X, Xiong S, Zheng B. Aurora Kinase A Regulates M1 Macrophage Polarization and Plays a Role in Experimental Autoimmune Encephalomyelitis. Inflammation. 2015;38(2):800–11.

9. Gilburt JAH, Girvan P, Blagg J, Ying L, Dodson CA. Ligand discrimination between active and inactive activation loop conformations of Aurora-A kinase is unmodified by phosphorylation. Chem Sci [Internet]. 2019;10(14):4069–76. Available from: http://dx.doi.org/10.1039/C8SC03669A

10. de Souza VB, Kawano DF. Structural basis for the design of allosteric inhibitors of the Aurora

kinase A enzyme in the cancer chemotherapy. Biochim Biophys Acta - Gen Subj [Internet]. 2020;1864(1):129448. Available from: https://doi.org/10.1016/j.bbagen.2019.129448

11. Richards MW, Burgess SG, Poon E, Carstensen A, Eilers M, Chesler L, et al. Structural basis of N-Myc binding by Aurora-A and its destabilization by kinase inhibitors. Proc Natl Acad Sci U S A. 2016;113(48):13726–31.

12. Ganapathi RN, Norris EJ, Sutker AP, Klotz KE, Ganapathi MK. Targeting Aurora A Kinase (AAK) in Platinum-Resistant High Grade Serous Ovarian Cancer. Front Oncol. 2020;10(August):1–9.

13. Beltran H, Oromendia C, Danila DC, Montgomery B, Hoimes C, Szmulewitz RZ, et al. A phase II trial of the aurora kinase a inhibitor alisertib for patients with castration-resistant and neuroendocrine prostate cancer: Efficacy and biomarkers. Clin Cancer Res. 2019;25(1):43–51.

14. Neumayer G, Belzil C, Gruss OJ, Nguyen MD. TPX2: Of spindle assembly, DNA damage response, and cancer. Cell Mol Life Sci [Internet]. 2014;71(16):3027–47. Available from: https://mcr.aacrjournals.org/content/1/4/271.full

15. Otto T, Horn S, Brockmann M, Eilers U, Schüttrumpf L, Popov N, et al. Stabilization of N-Myc Is a Critical Function of Aurora A in Human Neuroblastoma. Cancer Cell. 2009;15(1):67–78.

16. Zhao B, Smallwood A, Yang J, Koretke K, Nurse K, Calamari A, et al. Modulation of kinase-inhibitor interactions by auxiliary protein binding: Crystallography studies on Aurora A interactions with VX-680 and with TPX2. Protein Sci. 2008;17(10):1791–7.

17. Murray A. Cell cycle checkpoints. Curr Opin Cell Biol. 1994;6(6):872–6.

18. Eggert J. Genetics and Genomics in Oncology Nursing: What Does Every Nurse Need to Know? Nurs Clin North Am [Internet]. 2017;52(1):1–25. Available from: http://dx.doi.org/10.1016/j.cnur.2016.11.001

19. Fink DJ. Cancer Overview1. 1979;(JULY):2819–21.

20. Hanahan D, Weinberg RA. Hallmarks of cancer: The next generation. Cell [Internet]. 2011;144(5):646–74. Available from: http://dx.doi.org/10.1016/j.cell.2011.02.013

21. Balmain A, Brown K. Oncogene Activation in Chemical Carcinogenesis. Adv Cancer Res. 1988;51(C):147–82.

22. Alitalo K, Schwab M. Oncogene amplification in tumor cells. Adv Cancer Res. 1986;47(C):235–81.

23. Lingle WL, Lukasiewicz K, Salisbury JL. Deregulation of the centrosome cycle and the origin of chromosomal instability in cancer. Adv Exp Med Biol. 2005;570:393–421.

24. I. Evan G, H. Vousden K. Proliferation, cell cycle and apoptosis in cancer. Nature [Internet]. 2001;411(May):342–8. Available from: http://www.nature.com/nature/journal/v411/n6835/pdf/411342a0.pdf

25. Gorlova OY, Amos CI, Plaza OB. targets for cancer treatment. 2020;67–79.

26. Jones RG, Thompson CB. Tumor suppressors and cell metabolism: A recipe for cancer growth. Genes Dev. 2009;23(5):537–48.

27. Schwab M, Alitalo K, Klempnauer KH, Varmus HE, Bishop JM, Gilbert F, et al. Amplified DNA with limited homology to myc cellular oncogene is shared by human neuroblastoma cell lines and a neuroblastoma tumour. Nature. 1983;305(5931):245–8.

28. Look AT, Hayes FA, Shuster JJ, Douglass EC, Castleberry RP, Bowman LC, et al. Clinical relevance of tumor cell ploidy and N-myc gene amplification in childhood neuroblastoma: A pediatric oncology group study. J Clin Oncol. 1991;9(4):581–91.

29. Schneiderman AI, Braver ER, Kang HK. Understanding sequelae of injury mechanisms and mild traumatic brain injury incurred during the conflicts in Iraq and Afghanistan: persistent postconcussive symptoms and posttraumatic stress disorder. Am J Epidemiol. 2008;167(12):1446–52.

30. Schwab M, Alitalo K, Klempnauer KH, Varmus HE, Bishop JM, Gilbert F, et al. Understanding sequelae of injury mechanisms and mild traumatic brain injury incurred during the conflicts in Iraq and Afghanistan: persistent postconcussive symptoms and posttraumatic stress disorder. Am J Epidemiol. 1985;9(12):987–94.

31. Beltran H. The N-myc oncogene: Maximizing its targets, regulation, and therapeutic potential. Mol Cancer Res. 2014;12(6):815–22.

32. Phoenix TN, Gilbertson RJ. There's a Time and a Place for MYCN. Cancer Cell [Internet]. 2012;21(5):593–5. Available from: http://dx.doi.org/10.1016/j.ccr.2012.05.001

33. Huang M, Weiss WA. Neuroblastoma and MYCN. Cold Spring Harb Perspect Med. 2013;3(10).

34. Wada RK, Seeger RC, Brodeur GM, Einhorn PA, Rayner SA, Tomayko MM, et al. Human Neuroblastoma Cell Lines that Express N-myc without Gene Amplification. :3346–54.

35. Lu J, Lu B. The Ins and Outs of MYC Regulation by Posttranslational. 2006;281(46):34725–9.

36. Yan C, Higgins PJ. Biochimica et Biophysica Acta Drugging the undruggable : Transcription therapy for cancer. BBA - Rev Cancer [Internet]. 2013;1835(1):76–85. Available from: http://dx.doi.org/10.1016/j.bbcan.2012.11.002

37. Lambert SA, Jolma A, Campitelli LF, Das PK, Yin Y, Albu M, et al. Review The Human

Transcription Factors. Cell [Internet]. 2018;172(4):650–65. Available from: https://doi.org/10.1016/j.cell.2018.01.029

38. Fladvad M, Zhou K, Moshref A, Pursglove S, Ab B. N and C-terminal Sub-regions in the c-Myc Transactivation Region and their Joint Role in Creating Versatility in Folding and Binding. 2005;175–89.

39. Pineda-Lucena A, Ho CSW, Mao DYL, Sheng Y, Laister RC, Muhandiram R, et al. A Structure-based Model of the c-Myc/Bin1 Protein Interaction Shows Alternative Splicing of Bin1 and c-Myc Phosphorylation are Key Binding Determinants. J Mol Biol [Internet]. 2005 Aug;351(1):182–94. Available from: https://linkinghub.elsevier.com/retrieve/pii/S0022283605006017

40. Helander S, Montecchio M, Sears RC, Sunnerhagen M, Su Y, Kuruvilla J, et al. a Fuzzy Complex Regulates c-Myc Activity Article Pre-Anchoring of Pin1 to Unphosphorylated c-Myc in a Fuzzy Complex Regulates c-Myc Activity. 2015;1–13.

41. Nair SK, Burley SK. X-Ray Structures of Myc-Max and Mad-Max Recognizing DNA. Cell. 2003;112(2):193–205.

42. Posternak V, Cole MD. Strategically targeting MYC in cancer [version 1 ; referees : 2 approved] Referee Status : 2016;5:1–7.

43. Tu WB, Helander S, Pilstål R, Hickman KA, Lourenco C, Jurisica I, et al. Ubiquitin-Dependent Turnover of MYC Antagonizes MYC / PAF1C Complex Accumulation to Drive Transcriptional Elongation Article Ubiquitin-Dependent Turnover of MYC Antagonizes MYC / PAF1C Complex Accumulation to Drive Transcriptional Elongation. BBA - Gene Regul Mech [Internet]. 2014;1–14. Available from: http://dx.doi.org/10.1016/j.bbagrm.2014.06.002

44. Jaenicke LA, Carstensen A, Geyer M, Eilers M, Popov N, Eyss V, et al. Ubiquitin-Dependent Turnover of MYC Antagonizes MYC / PAF1C Complex Accumulation to Drive Transcriptional Elongation Article Ubiquitin-Dependent Turnover of MYC Antagonizes MYC / PAF1C Complex Accumulation to Drive Transcriptional Elongation. 2016;1–14.

45. Sjostrom SK, Finn G, Hahn WC, Rowitch DH, Kenney AM. The Cdk1 Complex Plays a Prime Role in Regulating N-Myc Phosphorylation and Turnover in Neural Precursors. 2005;9:327–38.

46. Farrell AS, Sears RC. MYC Degradation. Cold Spring Harb Perspect Med [Internet]. 2014 Mar 1;4(3):a014365–a014365. Available from: http://perspectivesinmedicine.cshlp.org/lookup/doi/10.1101/cshperspect.a014365

47. Blackwell TK, Huang J, Ma A, Kretzner L, Alt FW, Eisenman RN, et al. Binding of myc proteins to canonical and noncanonical DNA sequences. Mol Cell Biol [Internet]. 1993

Sep;13(9):5216–24. Available from: https://mcb.asm.org/content/13/9/5216.short

48. Dang C V. MYC on the Path to Cancer. Cell [Internet]. 2012 Mar;149(1):22–35. Available from: http://dx.doi.org/10.1016/j.cell.2012.03.003

49. Soucek L, Evan GI. NIH Public Access. 2011;20(1):1–8.

50. Jung LA, Gebhardt A, Koelmel W, Ade CP, Walz S, Kuper J, et al. OmoMYC blunts promoter invasion by oncogenic MYC to inhibit gene expression characteristic of MYC-dependent tumors. 2002;(February 2016):3507–10.

51. Beaulieu M-E, Jauset T, Massó-Vallés D, Martínez-Martín S, Rahl P, Maltais L, et al. Intrinsic cell-penetrating activity propels Omomyc from proof of concept to viable anti-MYC therapy. Sci Transl Med [Internet]. 2019 Mar 20;11(484):eaar5012. Available from: https://stm.sciencemag.org/lookup/doi/10.1126/scitranslmed.aar5012

52. Welcker M, Orian A, Jin J, Grim JA, Harper JW, Eisenman RN, et al. The Fbw7 tumor suppressor regulates glycogen synthase kinase 3 phosphorylation-dependent c-Myc protein degradation. Proc Natl Acad Sci [Internet]. 2004 Jun 15;101(24):9085–90. Available from: http://www.pnas.org/lookup/doi/10.1073/pnas.0402770101

53. Adhikary S, Eilers M. Transcriptional regulation and transformation by Myc proteins. Nat Rev Mol Cell Biol [Internet]. 2005 Aug;6(8):635–45. Available from: http://www.nature.com/articles/nrm1703

54. Soucek L, Whitfield J, Martins CP, Finch AJ, Murphy DJ, Sodir NM, et al. Modelling Myc inhibition as a cancer therapy. Nature [Internet]. 2008 Oct 17;455(7213):679–83. Available from: http://www.nature.com/articles/nature07260

55. Vader G, Lens SMA. The Aurora kinase family in cell division and cancer. Biochim Biophys Acta - Rev Cancer [Internet]. 2008 Sep;1786(1):60–72. Available from: https://linkinghub.elsevier.com/retrieve/pii/S0304419X08000310

56. Maris JM. Unholy Matrimony: Aurora A and N-Myc as Malignant Partners in Neuroblastoma. Cancer Cell [Internet]. 2009;15(1):5–6. Available from: http://dx.doi.org/10.1016/j.ccr.2008.12.008

57. Petersen J, Paris J, Willer M, Philippe M, Hagan IM. The S . pombe aurora-related kinase Ark1 associates with mitotic structures in a stage dependent manner and is required for chromosome segregation. 2001; Available from: http://jcs.biologists.org/content/114/24/4371.abstract

58. Kimura M, Matsuda Y, Yoshioka T, Okano Y. Cell Cycle-dependent Expression and Centrosome Localization of a Third Human Aurora/Ipl1-related Protein Kinase, AIK3. J Biol Chem [Internet]. 1999 Mar;274(11):7334–40. Available from: https://linkinghub.elsevier.com/retrieve/pii/S002192581837008X

59. Tanaka M, Ueda A, Kanamori H, Ideguchi H, Yang J, Kitajima S, et al. Cell-cycle-dependent Regulation of Human aurora A Transcription Is Mediated by Periodic Repression of E4TF1. J Biol Chem [Internet]. 2002 Mar;277(12):10719–26. Available from: https://linkinghub.elsevier.com/retrieve/pii/S0021925819362209

60. Nadler Y, Camp RL, Schwartz C, Rimm DL, Kluger HM, Kluger Y. Expression of Aurora A (but Not Aurora B) Is Predictive of Survival in Breast Cancer. 2008;14(14):4455–63.

61. Qi W, Cooke LS, Liu X, Rimsza L, Roe DJ, Manziolli A, et al. Aurora inhibitor MLN8237 in combination with docetaxel enhances apoptosis and anti-tumor activity in mantle cell lymphoma. Biochem Pharmacol [Internet]. 2011;81(7):881–90. Available from: http://dx.doi.org/10.1016/j.bcp.2011.01.017

62. Nu B, Dirks WG, Zehner R, Jr JC. Aurora Kinases as Targets in Drug-Resistant Neuroblastoma Cells. 2014;9(9):1–9.

63. Bischoff JR, Anderson L, Zhu Y, Mossie K, Ng L, Souza B, et al. A homologue of Drosophila aurora kinase is oncogenic and amplified in human colorectal cancers. 1998;17(11):3052–65.

64. Hutterer A, Berdnik D, Wirtz-Peitz F, Žigman M, Schleiffer A, Knoblich JA. Mitotic Activation of the Kinase Aurora-A Requires Its Binding Partner Bora. Dev Cell [Internet]. 2006 Aug;11(2):147–57. Available from: https://linkinghub.elsevier.com/retrieve/pii/S1534580706002589

65. Wittmann T, Wilm M, Karsenti E, Vernos I. Tpx2, a Novel Xenopus Map Involved in Spindle Pole Organization. J Cell Biol [Internet]. 2000 Jun 26;149(7):1405–18. Available from: https://rupress.org/jcb/article/149/7/1405/32046/Tpx2-a-Novel-Xenopus-Map-Involved-in-Spindle-Pole

66. Kufer TA, Silljé HHW, Körner R, Gruss OJ, Meraldi P, Nigg EA. Human TPX2 is required for targeting Aurora-A kinase to the spindle. J Cell Biol [Internet]. 2002 Aug 19;158(4):617–23. Available from: https://rupress.org/jcb/article/158/4/617/1141/Human-TPX2-is-required-for-targeting-AuroraA

67. Bhardwaj VK, Purohit R. Targeting the protein-protein interface pocket of Aurora-A-TPX2 complex: rational drug design and validation. J Biomol Struct Dyn [Internet]. 2020;0(0):000. Available from: http://dx.doi.org/10.1080/07391102.2020.1772109

68. Heidebrecht H, Adam-klages S, Szczepanowski M, Pollmann M, Buck F, Endl E, et al. repp86 : A Human Protein Associated in the Progression of Mitosis. 2003;1(February):271–9. Available from: https://mcr.aacrjournals.org/content/1/4/271.full

69. Eyers PA, Erikson E, Chen LG, Maller JL. A Novel Mechanism for Activation of the Protein Kinase Aurora A. 2003;13:691–7.

70. Zorba A, Buosi V, Kutter S, Kern N, Pontiggia F, Cho Y, et al. Molecular mechanism of Aurora A kinase autophosphorylation and its allosteric activation by TPX2. Elife [Internet]. 2014 May 27;3:1–24. Available from: https://elifesciences.org/articles/02667

71. Rowan FC, Richards M, Bibby RA, Thompson A, Bayliss R, Blagg J. Insights into aurora-A kinase activation using unnatural amino acids incorporated by chemical modification. ACS Chem Biol. 2013;8(10):2184–91.

72. Gustafson WC, Meyerowitz JG, Nekritz EA, Chen J, Benes C, Charron E, et al. Drugging MYCN through an Allosteric Transition in Aurora Kinase A, Supplemental Information. Cancer Cell. 2014;26(3).

73. Carmena M, Earnshaw WC. The cellular geography of Aurora kinases. Nat Rev Mol Cell Biol [Internet]. 2003 Nov;4(11):842–54. Available from: http://www.nature.com/articles/nrm1245

74. Martin MP, Zhu J, Lawrence HR, Pireddu R, Luo Y, Alam R, et al. 乳鼠心肌提取 HHS Public Access. ACS Chem Biol [Internet]. 2017;10(10):139–48. Available from: http://dx.doi.org/10.1039/C8SC03669A

75. McIntyre PJ, Collins PM, Vrzal L, Birchall K, Arnold LH, Mpamhanga C, et al. Characterization of Three Druggable Hot-Spots in the Aurora-A/TPX2 Interaction Using Biochemical, Biophysical, and Fragment-Based Approaches. ACS Chem Biol. 2017;12(11):2906–14.

76. Burgess SG, Grazia Concilio M, Bayliss R, Fielding AJ. Detection of Ligand-induced Conformational Changes in the Activation Loop of Aurora-A Kinase by PELDOR Spectroscopy. ChemistryOpen [Internet]. 2016 Dec 11;5(6):531–4. Available from: https://onlinelibrary.wiley.com/doi/10.1002/open.201600101

77. Keen N, Taylor S. Aurora-kinase inhibitors as anticancer agents. Nat Rev Cancer [Internet]. 2004 Dec;4(12):927–36. Available from: http://www.nature.com/articles/nrc1502

78. Lake EW, Muretta JM, Thompson AR, Rasmussen DM, Majumdar A, Faber EB, et al. Quantitative conformational profiling of kinase inhibitors reveals origins of selectivity for Aurora kinase activation states. Proc Natl Acad Sci U S A. 2018;115(51):E11894–903.

79. Orengo CA, Todd AE, Thornton JM. From protein structure to function. Curr Opin Struct Biol [Internet]. 1999 Jun;9(3):374–82. Available from: https://linkinghub.elsevier.com/retrieve/pii/S0959440X99800517

80. Thirumalai D, O'Brien EP, Morrison G, Hyeon C. Theoretical Perspectives on Protein Folding. Annu Rev Biophys [Internet]. 2010 Apr;39(1):159–83. Available from: http://www.annualreviews.org/doi/10.1146/annurev-biophys-051309-103835

81. Martin MP, Zhu J-Y, Lawrence HR, Pireddu R, Luo Y, Alam R, et al. A Novel Mechanism by

Which Small Molecule Inhibitors Induce the DFG Flip in Aurora A. ACS Chem Biol [Internet]. 2012 Apr 20;7(4):698–706. Available from: https://pubs.acs.org/doi/10.1021/cb200508b

82. Nussinov R, Tsai C, Shehu A, Jang H. Computational Structural Biology: Successes, Future Directions, and Challenges. Molecules [Internet]. 2019 Feb 12;24(3):637. Available from: http://www.mdpi.com/1420-3049/24/3/637

83. Hansson T, Oostenbrink C, van Gunsteren W. Molecular dynamics simulations. Curr Opin Struct Biol [Internet]. 2002 Apr;12(2):190–6. Available from: https://linkinghub.elsevier.com/retrieve/pii/S0959440X02003081

84. Jean-Quartier C, Jeanquartier F, Jurisica I, Holzinger A. In silico cancer research towards 3R. BMC Cancer [Internet]. 2018 Dec 12;18(1):408. Available from: https://bmccancer.biomedcentral.com/articles/10.1186/s12885-018-4302-0

85. Siebenmorgen T, Zacharias M. Computational prediction of protein–protein binding affinities. Wiley Interdiscip Rev Comput Mol Sci. 2020;10(3):1–18.

86. Creutz M, Freedman B. A statistical approach to quantum mechanics. Ann Phys (N Y) [Internet]. 1981 Apr;132(2):427–62. Available from: https://linkinghub.elsevier.com/retrieve/pii/0003491681900749

87. Rapp C, Kalyanaraman C, Schiffmiller A, Schoenbrun EL, Jacobson MP. A Molecular Mechanics Approach to Modeling Protein–Ligand Interactions: Relative Binding Affinities in Congeneric Series. J Chem Inf Model [Internet]. 2011 Sep 26;51(9):2082–9. Available from: https://pubs.acs.org/doi/10.1021/ci200033n

88. Petersen HG. Accuracy and efficiency of the particle mesh Ewald method. J Chem Phys [Internet]. 1995 Sep;103(9):3668–79. Available from: http://aip.scitation.org/doi/10.1063/1.470043

89. Tironi IG, Sperb R, Smith PE, van Gunsteren WF. A generalized reaction field method for molecular dynamics simulations. J Chem Phys [Internet]. 1995 Apr;102(13):5451–9. Available from: http://aip.scitation.org/doi/10.1063/1.469273

90. Grant BJ, Skjærven L, Yao XQ. The Bio3D packages for structural bioinformatics. Protein Sci. 2020;(July):1–11.

91. Maisuradze GG, Liwo A, Scheraga HA. Principal Component Analysis for Protein Folding Dynamics. J Mol Biol [Internet]. 2009 Jan;385(1):312–29. Available from: http://dx.doi.org/10.1016/j.jmb.2008.10.018

92. Djinovic-Carugo K, Carugo O. Missing strings of residues in protein crystal structures. Intrinsically Disord Proteins [Internet]. 2015 Jan 23;3(1):e1095697. Available from: https://www.tandfonline.com/doi/full/10.1080/21690707.2015.1095697

93. Kern D, Zuiderweg ERP. The role of dynamics in allosteric regulation. Curr Opin Struct Biol [Internet]. 2003 Dec;13(6):748–57. Available from: https://linkinghub.elsevier.com/retrieve/pii/S0959440X03001660

8. CURRICULUM VITAE